Available online at www.sciencedirect.com

ScienceDirect

Geochimica et Cosmochimica Acta xxx (2020) xxx–xxx

Geochimica et Cosmochimica Acta

www.elsevier.com/locate/gca

# Evidence for high organic carbon export to the early Cambrian seafloor

Meng Cheng [a], Chao Li [a,*], Chengsheng Jin [b], Haiyang Wang [a], Thomas J. Algeo [a,c,d], Timothy W. Lyons [e], Feifei Zhang [f], Ariel Anbar [g]

[a] State Key Laboratory of Biogeology and Environmental Geology, China University of Geosciences, Wuhan 430074, China
[b] Yunnan Key Laboratory for Palaeobiology, Yunnan University, Kunming 650091, China
[c] State Key Laboratory of Geological Process and Mineral Resources, China University of Geosciences, Wuhan 430074, China
[d] Department of Geology, University of Cincinnati, Cincinnati 45221-0013, USA
[e] Department of Earth Sciences, University of California, Riverside, CA 92521, USA
[f] School of Earth Sciences and Engineering, Nanjing University, Nanjing 210023, China
[g] School of Earth and Space Exploration, Arizona State University, Tempe 85287, USA

Received 20 March 2019; accepted in revised form 24 January 2020; available online xxxx

**Abstract**

Oxygenation of the early Cambrian ocean is commonly ascribed to high organic export to the sediment due to the rise of algae and filter-feeding animals, but direct evidence of elevated export fluxes has been lacking to date. Here, we report an integrated proxy dataset (U-Mo isotopes, Fe speciation, and major and trace elements) for lower Cambrian black shales at Yuanjia on the Yangtze Platform (South China). These shales are characterized by high iron speciation ratios and Mo and U enrichments, indicating persistently euxinic water conditions during their deposition, but a broad range of $\delta^{98}$Mo values (−0.10‰ to +1.94‰) implies strongly variable watermass sulfidity. High and variable nutrient element (Cu, Zn, Ni, Cd) enrichments at Yuanjia are consistent with elevated and variable organic productivity and export fluxes from the euphotic zone to the early Cambrian seafloor. The Yuanjia shales also exhibit super-heavy $\delta^{238}$U values (to +0.84‰) that cannot be explained by U reduction in sediment porewaters. We hypothesize that these values record a U reduction process within the water column, where U isotope fractionation can be much larger than in sediment porewaters. Such processes may have operated within a benthic organic flocculent layer at the sediment-water interface, a feature that is characteristic of high productivity systems with anoxic bottom waters. Furthermore, the coupling between $\delta^{238}$U, nutrient elements, and $\delta^{98}$Mo suggests that elevated productivity levels were driven likely by episodic upwelling in early Cambrian oceans, supplying abundant nutrients for productivity and influencing $H_2S$ concentrations in the water column. These observations, along with high organic carbon accumulation rates (5600 mg cm$^{-2}$ kyr$^{-1}$), are direct evidence of high organic export fluxes to the early Cambrian seafloor, thus providing key support for the hypothesis that enhanced organic export and burial triggered a major atmospheric-oceanic oxygenation event that stimulated the subsequent explosion of Cambrian life.


*Keywords:* U isotopes; Mo isotopes; Iron speciation; Flocculent layer; Primary productivity; Cambrian Explosion

## 1. INTRODUCTION

The early Cambrian was characterized by the rapid appearance of most phyla of modern animals and development of a modern-like marine ecosystem, an event known

* Corresponding author.
*E-mail address:* chaoli@cug.edu.cn (C. Li).

https://doi.org/10.1016/j.gca.2020.01.050
0016-7037/

as the "Cambrian Explosion" (Erwin et al., 2011). It began with the appearance of small shelly faunas near the base of the Cambrian Period (mainly in the Fortunian and Age 2; ~541–521 Ma) and culminated in the appearance of the complex animals of the Chengjiang Biota in Age 3 at ~518 Ma (Shu, 2008; Yang et al., 2018). The trigger for the Cambrian Explosion is inferred to have been a rapid increase in oxygen levels of the atmosphere-ocean system (Chen et al., 2015; Sperling et al., 2015b; Li et al., 2017), based in part on the idea that larger, more complex organisms have higher physiological requirements for oxygen than simple organisms (Sperling et al., 2015a). Concurrently, the evolution of primary producers and early animals during the Ediacaran-Cambrian periods may have changed oceanic carbon cycling and redox state as a result of biogeochemical and ecological feedbacks (Lenton et al., 2014; Li et al., 2018). Evidence from molecular fossils indicates a rapid rise of marine planktonic algae at ~659–645 Ma (Brocks et al., 2017), especially after the Marinoan Glaciation (van Maldegem et al., 2019). These algae replaced bacteria as the dominant marine primary producers, generating larger organic particulates that sank more rapidly through the water column, with an increase in the efficiency of organic carbon transport to the seafloor. The appearance of planktonic consumers (e.g., cnidarian jellyfish) also enhanced transport efficiency by packaging organic material in larger particles (Lenton et al., 2014). However, the biogeochemical effects of these events became apparent only after the biomass of filter-feeding organisms reached a critical level. Fossil evidence indicates that sponges underwent an explosive radiation during early Cambrian Ages 2–3 (e.g., the Niutitang sponge Lagerstätte, Fig. 1C) (Zhu, 2010), and that suspension-feeding mesozooplankton appeared in Cambrian Age 3 (Vinther et al., 2014). Thus, it seems likely that enhancement of the biological pump following the evolution of eukaryotic algae and planktonic consumers contributed to higher organic export fluxes to the early Cambrian seafloor and triggered oceanic oxygenation and the Cambrian Explosion.

Diverse types of geochemical evidence (e.g., iron speciation, redox-sensitive trace elements, and C-N-S-Mo-Cr-U isotopes) indeed support significant atmospheric and oceanic oxygenation during the Neoproterozoic-Cambrian transition, although no consensus has been reached concerning the nature of the rise (i.e., transient or permanent) and its role in driving the Cambrian Explosion (e.g., Och and Shields-Zhou, 2012; Chen et al., 2015; Li et al., 2017; Shi et al., 2018; Wang et al., 2018; Dahl et al., 2019). The accumulation of oxygen in the Earth-surface system is mainly due to burial of organic matter, and early Cambrian oceans are thought to have been organic matter sinks owing to the rise of algae and filter-feeding organisms that generated larger, more rapidly sinking organic particles (Logan et al., 1995; Brocks et al., 2017). However, direct evidence of high organic carbon export fluxes to the early Cambrian seafloor is lacking, so a key test of the "organic carbon burial hypothesis" for the Cambrian Explosion has not been undertaken to date.

Both Mo ($\delta^{98}$Mo) and U isotopes ($\delta^{238}$U) in organic-rich black shales have been used to track local and global redox conditions (e.g., Arnold et al., 2004; Wille et al., 2008; Dahl et al., 2010; Brennecka et al., 2011a; Dickson et al., 2014; Chen et al., 2015; Kendall et al., 2015). Their utility is based on behavioral variation of Mo and U in different redox conditions, i.e., conservative in oxic waters but reactive in anoxic (especially euxinic) environments, and on variable isotope fractionations between seawater and sediment during removal to the latter. Despite geochemical similarities, these two elements exhibit important differences, e.g., with regard to sites of sedimentary removal (i.e., water column or pore water), adsorption by organic matter and Fe-Mn oxides, and their response to the presence of $H_2S$. Therefore, paired use of Mo and U isotopes can potentially offer insights into the redox dynamics of ancient oceans that cannot be gained from either proxy by itself.

The $\delta^{238}$U of marine sediments also has the potential to provide insights into organic carbon fluxes to the seafloor. In anoxic settings with typical organic carbon sinking fluxes, reduction of U in sediment porewaters results in an isotopic fractionation ($\Delta^{238}U \leq 0.6‰$) relative to seawater $\delta^{238}$U (−0.39‰), yielding sediment $\delta^{238}U < +0.2‰$ (Andersen et al., 2014). However, an organic flocculent layer on the seafloor[*aka* a "fluff layer", as commonly in Black Sea literature, e.g., İzdar and Murray (1989)] may develop under conditions of elevated organic matter export from the surface ocean (Anderson et al., 1989). Although not yet confirmed experimentally, this layer was hypothesized to be capable of producing U isotope fractionations larger than those in sediment porewaters ($0.6‰ < \Delta^{238}U \leq \sim 1.2‰$), leading to abnormally high sediment $\delta^{238}$U (i.e., >+0.2‰) (Andersen et al., 2017); note that ~1.2‰ is the estimated maximum $\Delta^{238}$U (Bigeleisen, 1996; Abe et al., 2008).

To explore the conditions of organic carbon export to the seafloor in early Cambrian oceans, we generated an integrated geochemical dataset consisting of U isotope, Mo isotope, iron speciation, and major- and trace-element concentration data for organic-rich black shales of the lower Cambrian Niutitang Formation in the Yuanjia section—a typical slope-basinal setting on the southeastern margin of the early Cambrian Yangtze Platform, South China. Our data provide direct evidence supporting the hypothesis of enhanced organic matter export to the sediment in the early Cambrian ocean, thus providing a key link between contemporaneous atmospheric and oceanic oxygenation processes and bioevolutionary events.

## 2. GEOLOGICAL SETTING

During the late Ediacaran and earliest Cambrian, the South China Craton (SCC) was located at peri-equatorial paleolatitudes, proximal to the northwestern margin of Gondwana but not in contact with any continent (Fig. 1A) (Meert and Lieberman, 2008). The craton consisted of the Yangtze and Cathaysia blocks, which were separated by the failed intracratonic Nanhua rift basin. On the Yangtze Block, platform carbonates accumulated to the northwest and slope-basinal shales to the southeast (Zhu et al., 2003). As a result of eustatic transgression, the area of shale deposition peaked during Cambrian Ages 2–3,

Please cite this article in press as: Cheng M., et al. Evidence for high organic carbon export to the early Cambrian seafloor. *Geochim. Cosmochim. Acta* (2020), https://doi.org/10.1016/j.gca.2020.01.050

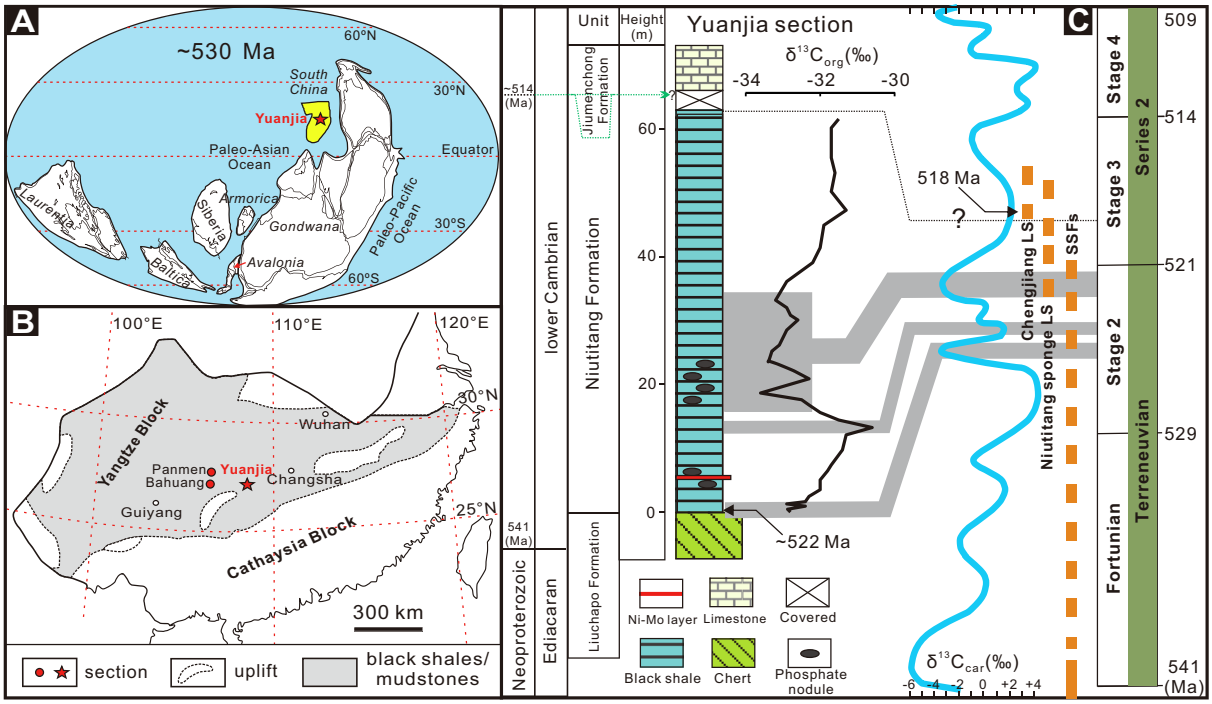


Fig. 1. Geological setting of the Yuanjia section. (A) Early Cambrian (~530 Ma) global paleogeography (Meert and Lieberman, 2008). (B) Paleogeography of South China Craton during early Cambrian Age 2–3 (Zhu et al., 2003). (C) Generalized stratigraphy of the Yuanjia section. The organic carbon $\delta^{13}C$ profile is from Guo et al. (2013); the carbonate $\delta^{13}C$ profile and biotic events are from Zhu et al. (2006). LS = Lagerstätte, SSF = small shelly fauna.

covering almost the entire Yangtze Platform (Fig. 1B) (Zhu et al., 2003).

The Yuanjia section is located in Zhongfang County, Hunan Province (27°29′25″N, 110°14′46″E). In this area, the uppermost Ediacaran-lower Cambrian succession consists of cherts of the Liuchapo Formation, black shales of the Niutitang Formation, and limestones of the Jiumenchong Formation (Fig. 1C). The Niutitang Formation contains >60 m of black shale with a Ni-Mo layer at its base and two phosphatic nodule layers in its lower half, representing typical slope-to-basinal deposits (Fig. 1C). Biostratigraphic data are not available for this section; however, a previous study placed the Precambrian/Cambrian boundary (541 Ma) within the upper Liuchapo Formation based on organic and inorganic carbon isotope correlations and SIMS zircon U-Pb dates (Fig. 1C) (Chen et al., 2015). The base of the Niutitang Formation has been dated at 522.3 ± 5.3 Ma and 522.3 ± 3.7 Ma (both SIMS U-Pb zircon ages) in the Panmen and Bahuang sections of Guizhou Province, respectively (Chen et al., 2015), which are ~120–130 km away from Yuanjia. The basal Ni-Mo layer has been dated at ~521 ± 5 Ma (a Re-Os isochron age) (Xu et al., 2011), constraining the onset of Niutitang black shale deposition to late Cambrian Age 2 (~529–521 Ma). The top of the Niutitang black shales at Yuanjia is most likely older than the ~518-Ma Chengjiang Biota based on organic and inorganic carbon isotope correlations (Fig. 1C) (Zhu et al., 2006). We estimate that the study interval at Yuanjia was deposited between ~522 and 518 Ma.

## 3. BACKGROUND OF GEOCHEMICAL PROXIES USED IN THIS STUDY

Iron speciation, now widely used as a redox proxy (reviewed by Poulton and Canfield, 2011), is defined in terms of the ratios of total Fe ($Fe_T$), pyrite ($Fe_{py}$), and highly reactive iron ($Fe_{HR}$)—the latter being the sum of Fe in pyrite, carbonate ($Fe_{carb}$), magnetite ($Fe_{mag}$), and oxides ($Fe_{ox}$). $Fe_{HR}/Fe_T$ values of <0.22 and >0.38 correspond to oxic-suboxic and anoxic bottom-water conditions, respectively, and when anoxia is indicated, $Fe_{py}/Fe_{HR}$ ratios of <0.7 and >0.8 correspond to ferruginous and euxinic conditions, respectively (Poulton and Canfield, 2011). A minimum $Fe_T$ value of 0.5% is required to avoid uncertainties in redox interpretations related to low Fe content, such as in carbonate-rich facies (Clarkson et al., 2014).

The behaviors of U and Mo are closely related to local watermass redox conditions. In oxic waters, both U and Mo are conservative although Mo has a high affinity for Mn oxides (Morford and Emerson, 1999). Adsorption of U onto Mn oxides is a function of seawater pH and carbonate and calcium ion concentrations; in normal seawater, the presence of U as soluble uranyl complexes inhibits the adsorption process (Wang et al., 2013). In oxygen-depleted waters, Mo and U are rapidly removed to the sediment (Tribovillard et al., 2006; Algeo and Tribovillard, 2009). Uranium uptake by the sediment depends on reduction of U(VI) to U(IV), which begins around the same potential that favors reduction of Fe(III) to Fe(II)—that is, in the near absence of dissolved oxygen but before the

Please cite this article in press as: Cheng M., et al. Evidence for high organic carbon export to the early Cambrian seafloor. *Geochim. Cosmochim. Acta* (2020), https://doi.org/10.1016/j.gca.2020.01.050

onset of sulfate reduction (often referred to as 'suboxic') (Tribovillard et al., 2006). In contrast, Mo uptake requires the presence of free $H_2S$ in order to convert molybdate ($MoO_4^{2-}$, the dominant species in oxic waters) to particle-reactive thiomolybdates ($MoO_{4-x}S_x^{2-}; x = 1-4$), with quantitative conversion occurring when aqueous [$H_2S$] is in excess of ~11 μM (25 , 1 atm and pH = 7–8) in a relatively restricted basin (Erickson and Helz, 2000; Dickson et al, 2014).

The isotopic composition of molybdenum ($\delta^{98}$Mo) in the sediment varies in response to different removal processes. Adsorption of Mo by Mn oxides results in an isotopic fractionation of ~−3‰ relative to seawater $\delta^{98}$Mo (+2.34‰ in the modern) (Barling and Anbar, 2004; Nakagawa et al., 2012). Similarly, $MoO_4^{2-}$ can be adsorbed by Fe oxides, resulting in variable isotopic fractionations ($-0.83 \pm 0.60$‰ to $-2.19 \pm 0.54$‰) depending on mineral speciation (Goldberg et al., 2009). Under sulfidic conditions,$MoO_4^{2-}$ is converted to thiomolybdate ($MoS_4^{2-}$), a process that goes to completion when [$H_2S$] exceeds the threshold of ~11 μM but that yields intermediate $MoO_{4-x}S_x^{2-}(x = 1-3)$ species at lower [$H_2S$] (Erickson and Helz, 2000). Complete conversion and quantitative precipitation of seawater Mo result in sediment $\delta^{98}$Mo being equal to contemporaneous seawater $\delta^{98}$Mo. Less than complete uptake of seawater Mo results in Mo-isotopic fractionations controlled by [$H_2S$], yielding variable sediment $\delta^{98}$Mo values generally between −0.7 and +2.3‰ (Poulson et al., 2006; Neubert et al., 2008). This process can be complicated by uptake of Mo by organic matter, which results in a negative isotopic fractionation of the adsorbed Mo (King et al., 2018).

Uranium isotopic fractionation varies depending on the pathway of U uptake by the sediment. In oxic seawater, Mn oxides preferentially adsorb isotopically light U, resulting in a fractionation of ~−0.2‰ relative to seawater (Brennecka et al., 2011b; Goto et al., 2014). Similarly, adsorption of U by goethite, birnessite, or illite produces an average fractionation of −0.15‰ (Jemison et al., 2016). Incorporation of U into primary carbonate phases results in no significant isotopic fractionation, but syndepositional diagenesis in anoxic porewaters can shift original values by +0.2 to +0.4‰ during U uptake by secondary carbonate precipitates (Romaniello et al., 2013; Chen et al., 2018). Laboratory experiments show that U reduction by sulfate- or metal-reducing microbes results in a large isotopic fractionation of +0.7 to +1.0‰, whereas abiotic U reduction via reductants such as $Fe^{2+}$ and aqueous $H_2S$ yields variable U isotope fractionations depending on aqueous U speciation and U reduction rate (Basu et al., 2014; Brown et al., 2018). Although the maximum U isotope fractionation observed in microbial reduction experiments is roughly consistent with the theoretical estimate of ~1.2‰ (Bigeleisen, 1996; Abe et al., 2008), observed fractionations in modern anoxic basins such as the Black Sea and Baltic Sea are significantly smaller (Andersen et al., 2014; Noordmann et al., 2015). This pattern has been explained as an effect of diffusion-limited U reduction in the sediment, limiting observed fractionations to a maximum of ~+0.6‰ and thus yielding maximum sediment $\delta^{238}$U of ~+0.2‰ relative to seawater $\delta^{238}$U of −0.39‰ (Andersen et al., 2014; Rolison et al., 2017).

Availability of nutrient elements (e.g., N, P, and Fe) controls marine productivity in the euphotic zone, and remineralization of organic matter replenishes nutrient inventories at depth (Schoepfer et al., 2015; Boyd et al., 2017; Weber et al., 2018). In anoxic (especially euxinic) waters, metal micronutrient elements (e.g., Cu, Zn, Ni, and Cd), which affect the synthesis of the enzymes relating to certain biochemical processes such as carbon fixation, are strongly removed to the sediment by incorporation into pyrite or formation of their own insoluble sulfides or by adsorption onto sedimentary organic matter (Tribovillard et al., 2006; Weber et al., 2018). Therefore, while the behaviors of these elements in seawater are closely linked to formation and decomposition of organic matter, their accumulation in the sediment is also influenced by local redox conditions (Tribovillard et al., 2006). For these reasons, paleoproductivity can be tracked accurately only if local redox conditions have been independently reconstructed. In this study, we use iron speciation and Mo isotope data as independent proxies for water-column redox conditions.

## 4. MATERIALS AND METHODS

A total of 27 samples were collected from a fresh outcrop on a newly constructed road near Yuanjia village, Huaihua City, Hunan Province, China (27°29′25″N, 110° 14′46″E). Portions of the outcrop showing visible veins or macroscopic pyrite were avoided, and the outer part of each sample was trimmed off in the laboratory, leaving the least altered core of each sample (~50 g). This material was crushed to powder (>200 mesh) for geochemical analysis. Total organic carbon (TOC), iron speciation, and major elements were analyzed in the State Key Laboratory of Biogeology and Environmental Geology in the China University of Geosciences (Wuhan), and trace elements, Mo isotope and U isotope are analyzed in W.M. Keck Foundation Laboratory at Arizona State University.

For measurement of TOC concentrations, ~2 g of sample powder was weighed into a glass container, and 4 mol $L^{-1}$ HCl was added to dissolve carbonate. After complete carbonate dissolution, the residuum was centrifuged, neutralized to pH = 7, and dried. Then, ~20 mg of treated powder was weighed into a C-S analyzer (Analytic Jena, multi EA 4000) and analyzed with a reproducibility better than 0.2 wt%.

For major elements, 0.6 g of sample powder was mixed with 6 g $Li_2B_4O_7$, heated to 1080 °C, and made into a glass disk. Then, the glass disk was analyzed with a Panalytical Epsilon 3 X-ray Fluorescence (XRF) spectrometer with an analytical precision better than 5% (based on long-term analysis on standard GSR-5).

A sequential extraction method was used for iron associated with carbonate ($Fe_{carb}$), reducible oxides ($Fe_{ox}$), and magnetite ($Fe_{mag}$) (Poulton and Canfield, 2005), and an improved $CrCl_2$ reduction method was used for pyrite-hosted iron ($Fe_{py}$) (Li et al., 2015). The data quality was monitored by repeated analysis of standards from Timothy

Please cite this article in press as: Cheng M., et al. Evidence for high organic carbon export to the early Cambrian seafloor. *Geochim. Cosmochim. Acta* (2020), https://doi.org/10.1016/j.gca.2020.01.050

Lyons's laboratory at University of California-Riverside (USA), with a reproducibility generally better than 0.1% (Li et al., 2015).

For trace element, Mo isotope and U isotope measurements, a mixture of HF, $HNO_3$ and HCl acids were used to fully digest an aliquot of each sample. Then, the solution was diluted with 2% $HNO_3$ and measured on a Thermo Fisher iCAP Q inductivity coupled plasma mass spectrometer (ICP-MS) with a precision generally better than 5%, based on repeated analysis of in-run check standards. Then, digested solutions containing ~250 ng Mo and ~125 ng U were transferred to a new Teflon beaker and separately mixed with a double-spike solution ($^{97}$Mo-$^{100}$Mo for Mo, and $^{233}$U-$^{236}$U for U). Cation resin (50WX-8) and anion resin (AG1X-8) were used to separate Mo from the matrix, while UTEVA resin was used to separate U from the matrix. The details of the protocols for chemical purifications are given in Anbar et al. (2001) and Weyer et al. (2008). The separated solutions were analyzed for Mo and U isotopes on a Thermo Fisher Neptune multi-collector ICP-MS (MC-ICP-MS). Every sample was run three times for Mo isotopes and two times for U isotopes, with the results reported as an average value (±2 SD) in per mille deviation relative to a standard. Mo isotope results were determined relative to the RochMo2 standard (Johnson Matthey Specpure® Mo plasma standard, Lot #802309E) and recalculated to NIST SRM 3134 as $\delta^{98}$Mo (or $\delta^{98/95}$Mo) = [$\delta^{98/95}Mo_{sample}/(\delta^{98/95}Mo_{standard}$ - × 0.99975) − 1] × 1000. Relative to NIST SRM 3134, RochMo2 yields a $\delta^{98/95}$Mo composition of −0.08 ± 0.05‰ (Goldberg et al., 2013; Nägler et al., 2013). During four days of Mo isotope analysis for this study, SDO-1 yielded an average value of 1.13 ± 0.02‰ (2SD; $n = 15$) relative to NIST SRM 3134 (0.25‰), which is close to the value obtained in earlier studies (1.05 ± 0.14‰ and 1.08 ± 0.15‰) (Goldberg et al., 2013; Kendall et al., 2015). Uranium isotope results are reported relative to CRM145 as $\delta^{238}$U (or $\delta^{238/235}$U) = [$\delta^{238/235}U_{sample}/\delta^{238/235}U_{CRM145} - 1$] × 1000. Repeated analysis of CRM145 yielded a mean of 0.00 ± 0.07‰ (2SD; $n = 135$). CRM129a, which was used to monitor data quality, yielded an average value of −1.68 ± 0.05‰ (2SD; $n = 14$) during the analytical period, consistent within external uncertainty with the value (−1.72 ± 0.09‰) reported by Kendall et al. (2015).

Organic carbon accumulation rates (OCAR) were calculated per the protocol of Algeo et al. (2013):

$$OCAR = [TOC] \times BAR \quad (1)$$

where [TOC] is total organic carbon concentration, and BAR is bulk accumulation rate.

$$BAR = \rho \times LSR \quad (2)$$

where $\rho$ refers to the sediment dry bulk density in unit of g cm$^{-3}$, and LSR refers to a linear sedimentation rate (in unit of cm kyr$^{-1}$) which is calculated with a series of biostratigraphically or radiometrically dated tie points, between each pair of which sedimentation rates are assumed to be linear. In this study, since the ρ data was not available, we used a constant typical value of 2.5 g cm$^{-3}$ for all samples (Algeo et al., 2013). Based on the 64 m thickness of the study section and lower and upper boundary ages of 522 Ma and 518 Ma (see Section 2), its average LSR is ~1.6 cm kyr$^{-1}$.

Enrichment factors (EFs) were calculated relative to the upper continental crust (UCC) as follows: $X_{EF} = (X/Al)_{sample}/(X/Al)_{UCC}$, where X refers to the element of interest (e.g., Mo or U), and elemental concentrations for UCC are from McLennan (2001).

## 5. RESULTS

All geochemical data generated in this study are given in Supplementary Table S1, with key results illustrated in Figs. 2 and 3.

### 5.1. Iron speciation, Mo and U concentrations

Almost all samples at Yuanjia yield $Fe_{HR}/Fe_T > 0.38$ and $Fe_{py}/Fe_{HR} > 0.7$ (mostly > 0.8) (Fig. 2), indicating mainly euxinic bottom-water conditions during deposition, consistent with prior inferences that euxinia was prevalent at mid-depths of the Nanhua Basin during the early Cambrian (e.g., Feng et al., 2014; Jin et al., 2016; Li et al., 2017). The two samples of NTT-26 at 25.2 m and NTT-48 at 46.2 m yield $Fe_{HR}/Fe_T > 0.38$ but $Fe_{py}/Fe_{HR} < 0.7$. Because these two samples have $Fe_T < 0.5\%$ (Fig. 2), we consider these ratios are unreliable. Mo and U show high EFs [MoEF: 19-771, mean 225 ± 201; UEF: 6–194, mean 44 ± 43 (±1SD)], consistent with the euxinic bottom-water conditions inferred by coexisting iron speciation data.

### 5.2. TOC and nutrient metal elements

The TOC is high, ranging from 6.4% to 35.5%, and shows a decreasing trend upsection, except for samples at 46.2 m (26.1%) and 46.7 m (35.5%). Enrichments of Cu, Ni, Zn, and Cd are generally high ($Cu_{EF}$: 24 ± 37; $Zn_{EF}$: 20 ± 40; $Ni_{EF}$: 14 ± 14; $Cd_{EF}$: 406 ± 786) (mean ± 1SD) even comparing to those in typical modern high-productivity region, such as the Peru upwelling margins ($Cu_{EF}$: 5 ± 2; $Zn_{EF}$: 3 ± 1; $Ni_{EF}$: 4 ± 3; $Cd_{EF}$: 544 ± 505) (Böning et al., 2004), and also show a general decrease upsection ($Cu_{EF}$: 196 to 1.3; $Zn_{EF}$: 166 to 0.4; $Ni_{EF}$: 74 to 2.0; $Cd_{EF}$: 3028 to 3.1), although substantial variability is observed in all profiles (Fig. 3). Strong positive correlations exist between these nutrient metal elements, with the square of correlation coefficient ($R^2$) ranging from 0.40 for Cu vs. Ni to 0.95 for Cd vs. Zn (both $p < 0.01$, $n = 29$) (Fig. 4A and B).

### 5.3. Mo and U isotopes

To avoid the influence of detritally sourced Mo and U, we calculated the isotopic composition of the authigenic Mo and U fractions by adopting UCC $\delta^{98}$Mo (=0‰) and $\delta^{238}$U (=−0.3‰) as the isotopic compositions of their detrital fractions (cf. Andersen et al., 2018). Due to the high EFs for both Mo and U, there are only limited differences between their bulk isotopic compositions [range 0–0.03‰, mean 0.01 ± 0.03‰ (2SD) for Mo; range 0–0.14‰, mean

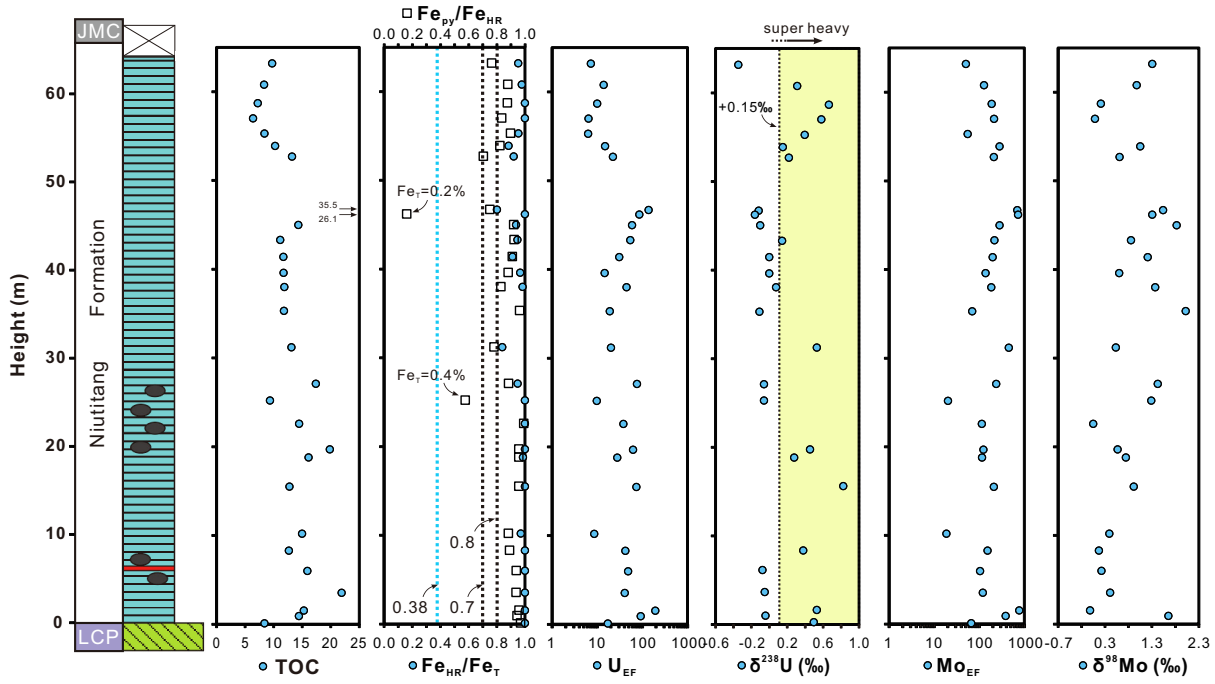


Fig. 2. Chemostratigraphy of lower Cambrian Yuanjia section. The vertical line (+0.15‰) in the $\delta^{238}U$ profile represents the threshold value for reduction of U in benthic flocculent layers, and the vertical lines (0.38, 0.70 and 0.80) in the Fe-ratio profile represent key threshold values of Fe speciation proxies. See text for more details.

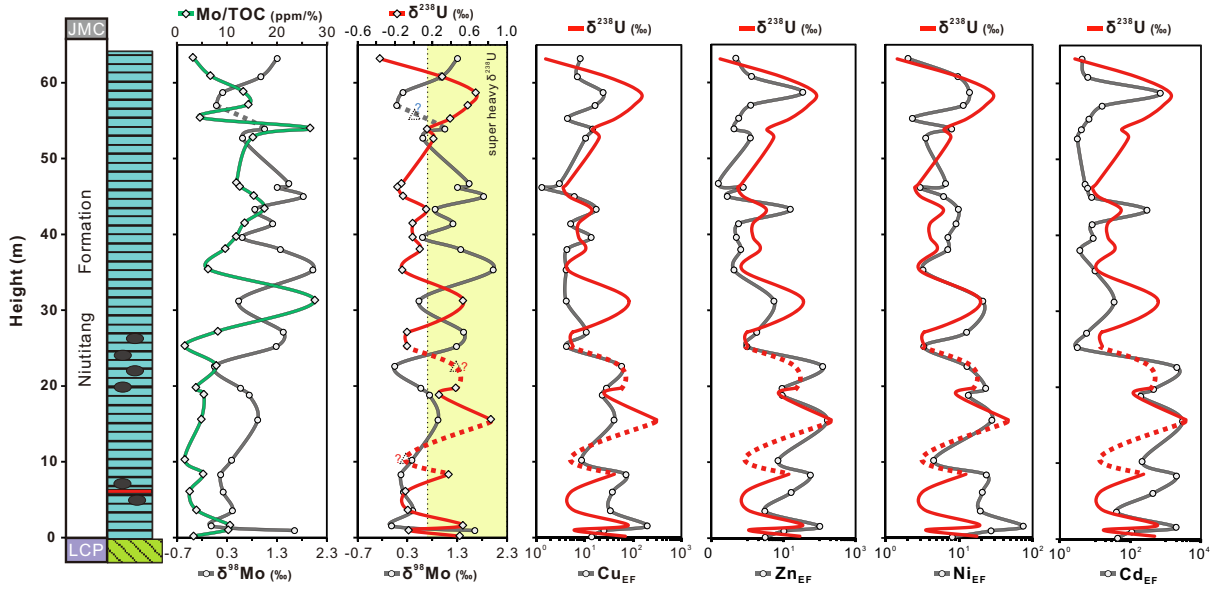


Fig. 3. Stratigraphic coupling of key geochemical proxies in the lower Cambrian Yuanjia section. The negative coupling of $\delta^{98}Mo$ with Mo/TOC indicates a local rather than global redox control on their variations. The positive couplings between nutrient metals and $\delta^{238}U$ suggest that enhanced productivity was a key factor in formation of organic flocculent layers on the early Cambrian seafloor at Yuanjia. See text for more details.

$0.03 \pm 0.07$‰ (2SD) for U]. Henceforth, unless otherwise specified, all isotopic values refer to the authigenic fraction.

Sediment $\delta^{98}Mo$ values at Yuanjia show high degree of stratigraphic variability ranging from −0.10‰ to +1.94‰, which are variably lower than the modern seawater value of +2.34‰, but similar to data from other lower Cambrian sections in South China (Chen et al., 2015; Wen et al., 2015; Cheng et al., 2016, 2017).

Sediment $\delta^{238}U$ values at Yuanjia range from −0.34 to +0.84‰. In modern anoxic basins, sediment $\delta^{238}U$ is generally not higher than +0.2‰ (Fig. 5) (e.g., Andersen et al., 2014; Rolison et al., 2017), representing a maximum

Please cite this article in press as: Cheng M., et al. Evidence for high organic carbon export to the early Cambrian seafloor. *Geochim. Cosmochim. Acta* (2020), https://doi.org/10.1016/j.gca.2020.01.050

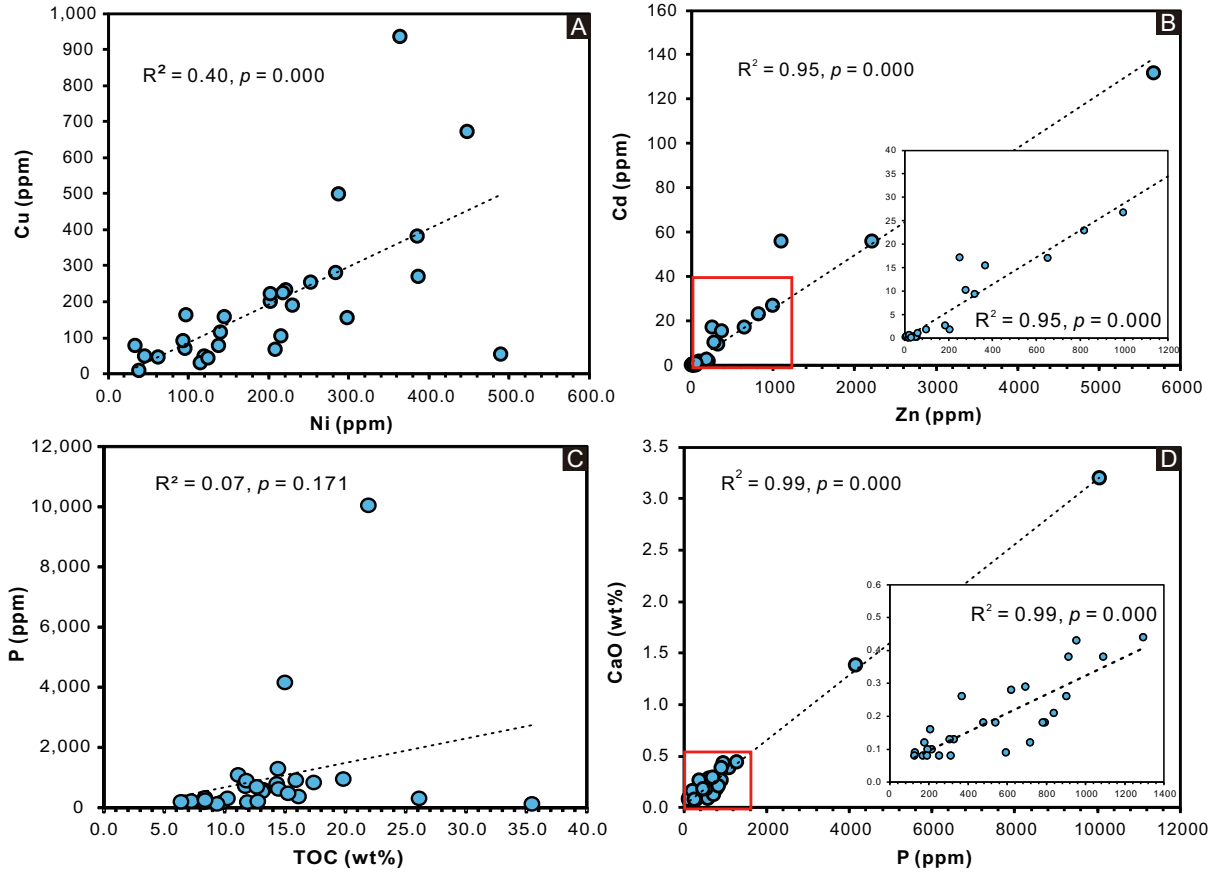


Fig. 4. Crossplots of Cu versus Ni (A), Cd versus Zn (B), P versus TOC (C), and CaO versus P (D) for the Yuanjia section. The inserts in B and D are the close looks of the areas in red rectangles in B and D.

fractionation of ~+0.6‰ relative to seawater $\delta^{238}U$, which is significantly less than the maximum theoretical $\Delta^{238}U$ of ~+1.2‰ (Andersen et al., 2014). This limited fractionation has been attributed to U reduction occurring mainly in porewaters containing only small amounts of dissolved U. Furthermore, the study by Dahl et al. (2017) from Siberia inferred that early Cambrian (~520 Ma) seawater $\delta^{238}U$ was lower (−0.65‰ to −0.45‰) than that of the modern ocean (−0.39‰). If correct, then at least 14 out of 27 $\delta^{238}U$ values at Yuanjia correspond to an isotopic fractionation larger than ~+0.6‰ (i.e., >+0.15‰), with some values being close to the maximum theoretical fractionation of ~1.2‰.

A moderate negative correlation is observed between $\delta^{238}U$ and $\delta^{98}Mo$ ($R^2 = 0.40$, $p < 0.01$; Fig. 6A). Additionally, $\delta^{238}U$ shows positive covariations with the EFs of Cu, Zn, Ni and Cd. The correlations are fairly obvious in chemostratigraphic profiles (Fig. 3) but become statistically insignificant when crossplotted for the study section as a whole (not shown). This situation arises because the correlations are strongest over local stratigraphic intervals (probably reflecting a single dominant control), whereas at the scale of the full study section the influence of multiple controls results in a weaker relationship. To demonstrate the strength of local stratigraphic correlations, we calculated correlation coefficients (r) for five-point moving windows through the full study section, yielding values of <−0.5 or >0.5 for most of the section (Fig. 7).

## 6. DISCUSSION

### 6.1. Basin connection with open ocean

Mo-U relationships can be useful for assessment of basinal watermass dynamics (Algeo and Tribovillard, 2009). The Yuanjia black shales were deposited under mainly euxinic conditions, as indicated by iron speciation data and Mo-U enrichments (see Section 5.1; Fig. 2), which are favorable for the formation of pyrite and the accumulation of authigenic Mo. Owing to rapid removal of Mo to the sediment, the concentration of aqueous Mo in a restricted basin can become strongly reduced through time, leading to a "flat" Mo-U trend (Fig. 6B). For example, Mo in deep waters of the modern Black Sea is ~97% depleted relative to normal seawater, whereas aqueous U exhibits a much smaller degree of depletion (~40%) (Algeo and Lyons, 2006; Rolison et al., 2017). Authigenic Mo and U enrichments in Yuanjia shales show no evidence of differential depletion, and the normal-marine-like Mo/U ratios are evidence that the early Cambrian Nanhua Basin was connected to the open ocean (Fig. 6B). However, it should be noted that a semi-restricted condition (e.g., as for the

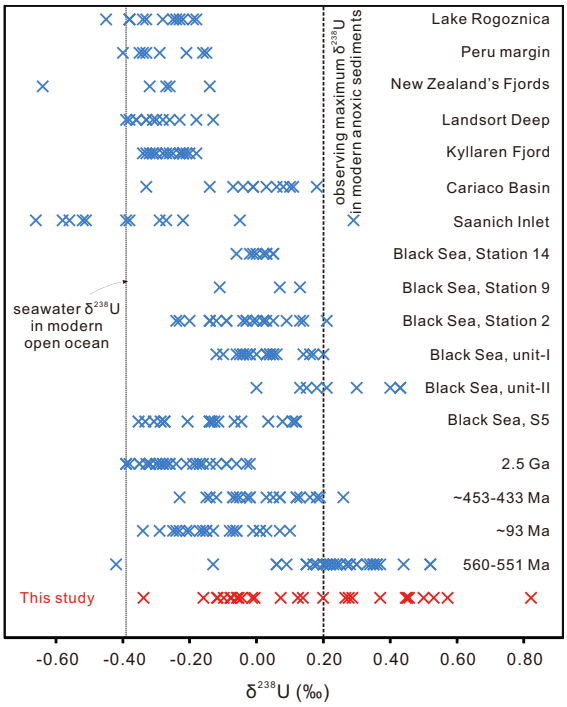


Fig. 5. Compilation of $\delta^{238}U$ data for modern anoxic basins, ancient black shales, and the Yuanjia section. Generally, most modern anoxic black shales yield $\delta^{238}U < +0.2‰$, corresponding to an isotopic fractionation of $<\sim 0.6‰$ in porewaters. In contrast, $\delta^{238}U$ data from Black Sea Unit II as well as the lower Cambrian Yuanjia section show much higher values, which we attribute to U reduction in a benthic flocculent layer. Data sources: Lake Rogoznica: Bura-Nakić et al. (2018), Peru Margin: Weyer et al. (2008), New Zealand fjords: Hinojosa et al. (2016), Landsort Deep: Noordmann et al. (2015), Kyllaren Fjord: Noordmann et al. (2015), Cariaco Basin: Andersen et al. (2014), Saanich Inlet: Holmden et al. (2015), Black Sea Station 14: Andersen et al. (2014), Black Sea Station 9: Andersen et al. (2014), Black Sea Station 2: Rolison et al. (2017), Black Sea Unit I: Montoya-Pino et al. (2010), Black Sea Unit II: Montoya-Pino et al. (2010), Black Sea S5: Andersen et al. (2018), 2.5 Ga: Kendall et al. (2013), ~453–433 Ma: Lu et al. (2017), 560–551 Ma: Kendall et al. (2015), ~93 Ma: Montoya-Pino et al. (2010).

modern Cariaco Basin or Saanich Inlet) will not be apparent on a $Mo_{EF}$-$U_{EF}$ crossplot, so partial restriction of the early Cambrian Nanhua Basin cannot be precluded.

### 6.2. Variable bottom-water sulfidity

As introduced in Section 3, $\delta^{98}Mo$ in black shales has the potential to record global seawater $\delta^{98}Mo$ when the local bottom-water $[H_2S]$ exceeds the threshold value ($\sim$11 μM) (Arnold et al., 2004; Neubert et al., 2008; Wille et al., 2008; Dickson, 2017). However, several considerations show that the observed $\delta^{98}Mo$ values at Yuanjia reflect dominantly local controls. First, many $\delta^{98}Mo$ values are lower than +0.7‰, the best available estimate for average riverine $\delta^{98}Mo$ (Archer and Vance, 2008), and lower even than continental crustal values of 0–0.4‰ (Voegelin et al., 2014). Since Mo isotopic fractionation during magmatism (Voegelin et al., 2014; Yang et al., 2017), weathering (Gardner et al., 2017), and transport (Archer and Vance, 2008) is limited, Cambrian riverine $\delta^{98}Mo$ should have been close to the modern value (although there are no relevant data at present). These low $\delta^{98}Mo$ values cannot record contemporaneous seawater $\delta^{98}Mo$, which must have been equal to or greater than riverine $\delta^{98}Mo$ owing to a lack of any known process that preferentially removes the heavy isotope ($^{98}Mo$) from seawater. Second, seawater $\delta^{98}Mo$ is relatively stable owing to the long residence time of Mo in seawater ($\sim$0.5 Myr for the modern ocean and probably similar for the Cambrian) (Chen et al., 2015). Thus, the high degree of stratigraphic variability in $\delta^{98}Mo$ at Yuanjia, corresponding to time scale less than the Mo residence time, is inconsistent with a seawater $\delta^{98}Mo$ signal (Kendall et al., 2017). Third, $\delta^{98}Mo$ at Yuanjia shows a generally negative correlation with Mo/TOC (Fig. 3), a proxy used to track the size of the aqueous Mo reservoir (Algeo and Lyons, 2006). If the Yuanjia black shales had captured the contemporaneous seawater $\delta^{98}Mo$ signal, then a positive correlation should have been produced because both a larger marine Mo inventory and more positive $\delta^{98}Mo$ values are expected for times of greater marine oxygenation, and vice versa (Kendall et al., 2017).

A number of local processes can cause Mo isotope fractionation and variable sediment $\delta^{98}Mo$. In some samples with low $\delta^{98}Mo$, Mo enrichment significantly exceeds that of U (Fig. 6B), which implies operation of a Fe-Mn shuttle whereby isotopically light Mo was preferentially adsorbed by Fe-Mn oxides and transferred to the sediment (Algeo and Tribovillard, 2009; Cheng et al., 2016). Fe-Mn oxides adsorb aqueous Mo above the chemocline and release it back to the water column below the chemocline (Algeo and Tribovillard, 2009). Adsorption of U to Mn oxides is strong at low pH (2.5–3), but it becomes much weaker above circum-neutral pH due to formation of stable uranyl-carbonate aqueous complexes that do not readily absorb onto particulates (Wang et al., 2013). Mo that is captured by a Fe-Mn particulate shuttle can be transferred to the sediment, leading to higher enrichments of Mo relative to U (Algeo and Tribovillard, 2009). This process operates most vigorously in weakly euxinic settings in which the $O_2$-$H_2S$ chemocline fluctuates dynamically just above or across the sediment-water interface (Algeo and Tribovillard, 2009; Cheng et al., 2016). In this circumstance, the transition of $MoO_4^{2-}$ to $MoS_4^{2-}$ via $MoO_{4-x}S_x^{2-} (x = 1-3)$ is accompanied by a large isotope fractionation, the degree of which is a function of $[H_2S]$ (Erickson and Helz, 2000). This operation of a Fe-Mn shuttle suggests that at least some samples from Yuanjia were deposited in weakly euxinic waters with $[H_2S]$ lower than the threshold for quantitative Mo conversion from $MoO_4^{2-}$ to $MoS_4^{2-}$. This circumstance, as well as the operation of an Fe-Mn shuttle, can account for the relatively lower $\delta^{98}Mo$ values. Additionally, under weakly euxinic conditions, adsorption of Mo by organic matter is enhanced, which also produces a fractionation favoring the light Mo isotope (King et al., 2018). However, there is no obvious correlation between $\delta^{98}Mo$ and TOC at Yuanjia ($R^2 = 0.03$; Fig. 6C). This is consistent with our argument

Please cite this article in press as: Cheng M., et al. Evidence for high organic carbon export to the early Cambrian seafloor. *Geochim. Cosmochim. Acta* (2020), https://doi.org/10.1016/j.gca.2020.01.050

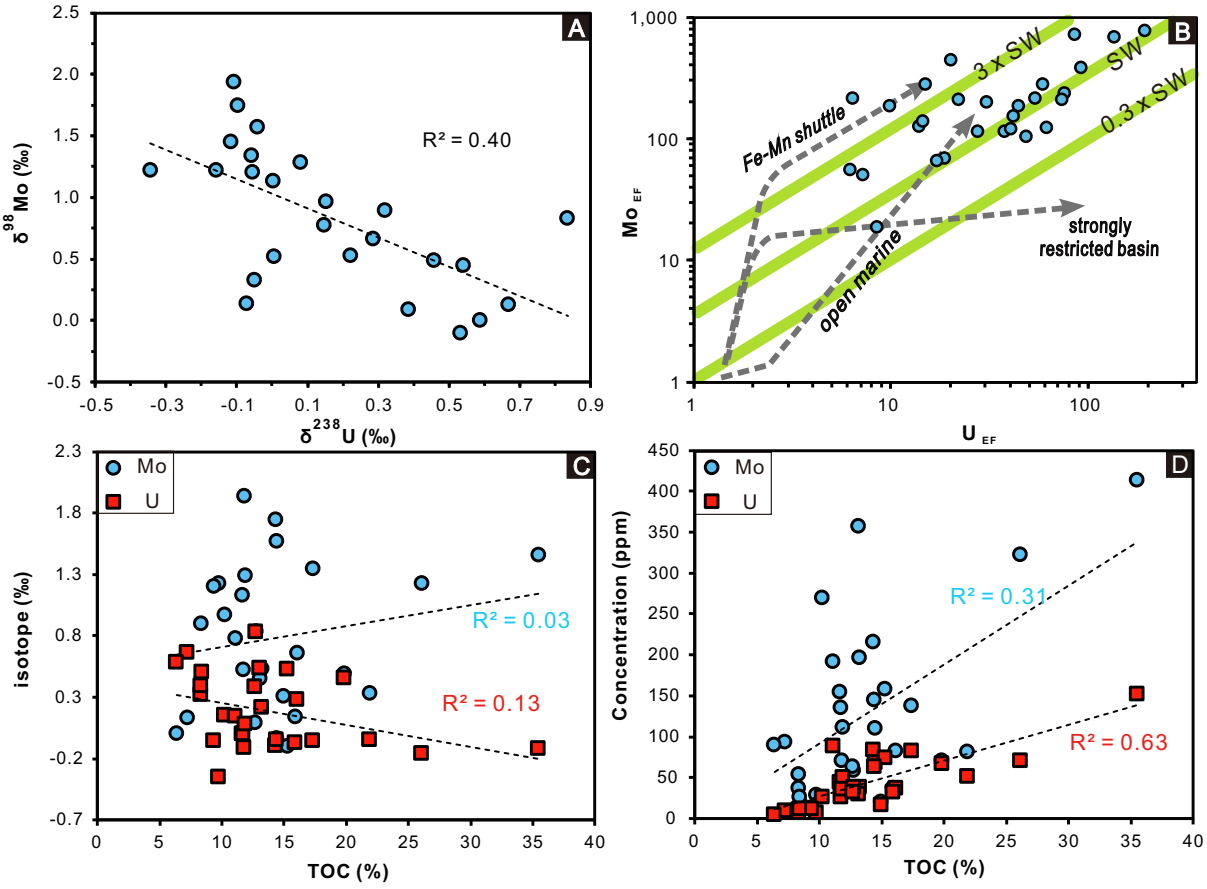


Fig. 6. Crossplots of $\delta^{238}U$ versus $\delta^{98}Mo$ (A), Mo enrichment factor ($Mo_{EF}$) versus U enrichment factor ($U_{EF}$) (B), TOC versus $\delta^{98}Mo$ and $\delta^{238}U$ (C), and TOC versus Mo and U concentrations (D). B is modified after Algeo and Tribovillard (2009).

that local sulfidity was variable, and that relatively lighter $\delta^{98}Mo$ values were due to a combination of low [$H_2S$], operation of an Fe-Mn shuttle, and adsorption by organic matter. Since the latter two processes are favored by low [$H_2S$] conditions, we infer that lower and higher $\delta^{98}Mo$ values correspond to lower and higher [$H_2S$], respectively, although this relationship was not necessarily linear.

### 6.3. High and variable paleoproductivity

Primary productivity in the photic zone generates organic matter that sinks through the water column and is, in part, buried in the sediment (Breitburg et al., 2018). Accompanying this process, nutrients and other elements can be incorporated into or adsorbed onto organic matter and released back to the water column or pore waters during organic decomposition. Elements that are released into pore waters can be captured by pyrite or other authigenic minerals (Tribovillard et al., 2006). In euxinic waters, Cd tends to form its own sulfide, whereas Zn, Cu, and Ni are commonly incorporated into pyrite, although all of these elements can be also associated with organic matter (Algeo and Maynard, 2004; Large et al., 2014). However, the limited correlations of these elements with TOC ($r < 0.30$; not shown) at Yuanjia indicate that sedimentary organic matter is not their primary host phase. These elements may likely reside mainly in authigenic phases, the formation of which depends heavily on local bottom-water conditions. At Yuanjia, the micronutrients Cu, Ni, Zn, and Cd yield similar chemostratigraphic profiles, with $R^2$ ranging from 0.40 for Cu vs. Ni to 0.95 for Cd vs. Zn (both $p < 0.05$, $n = 29$) (Fig. 4A and B). They also show negative correlation with $\delta^{98}Mo$ (Fig. 3), suggesting greater enrichment of these micronutrient elements under less reducing conditions (see above), which is inconsistent with a dominant redox control on their sedimentary enrichment. In addition, no obvious variations in lithology or grain size were observed in the study section, suggesting that variations in Cu, Zn, Ni, and Cd concentrations were not controlled by sedimentation rate. The strong correlations between these elements are thus probably indicative of a common source in the organic sinking flux, which is closely linked to primary productivity rates, rather than in the formation of authigenic phases (e.g., pyrite). Since the bottom waters at Yuanjia were persistently euxinic (Section 6.1), $H_2S$ was in excess for formation of sulfide minerals. Therefore, we infer that the stratigraphic variations of these nutrient elements most likely reflect changes in primary and export productivity at the study site. Accordingly, the high and variable enrichments of these nutrients support

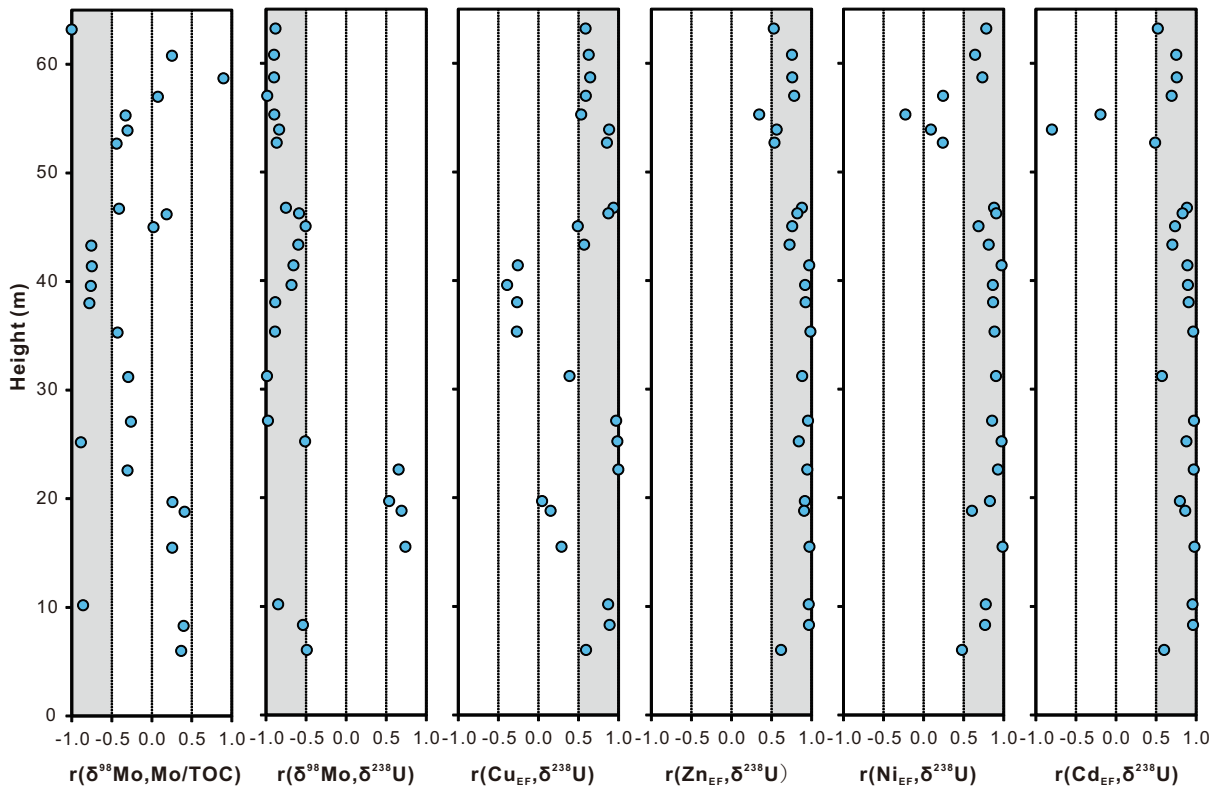


Fig. 7. Correlation coefficients (r) for pairs of geochemical proxies using a five-point moving window through the Yuanjia section. The gray areas highlight significant correlations.

elevated and variable organic productivity and export fluxes from the euphotic zone to the early Cambrian seafloor.

It should be noted that stratigraphic variations of Cu, Zn, Ni and Cd are not consistent with those of P or Ba, which are widely used as paleoproductivity proxies (Schoepfer et al., 2015). P concentration is a reliable productivity proxy when it correlates positively with TOC (Schoepfer et al., 2015), but this was not observed at Yuanjia ($R^2 = 0.07$, $p > 0.05$, $n = 29$) (Fig. 4C). Instead, P may be present in the sediment mainly as authigenic apatite since a strong positive correlation between P and CaO is observed ($R^2 = 0.99$, $p < 0.05$) (Fig. 4D). Actually, P concentration is not expected as a robust productivity proxy in euxinic deposits such as the Yuanjia black shale as it can be regenerated back to seawater (Schoepfer et al., 2015). Ba is commonly delivered to the sediment as barite precipitated on the surface of sinking, decaying organic particles, but it is unstable in euxinic pore waters and can undergo reductive dissolution, releasing Ba back to the water column (Tribovillard et al., 2006). Therefore, Ba concentrations may not be reliable as a paleoproductivity proxy in the dominantly euxinic Yuanjia section. Furthermore, high Ba concentrations in lower Cambrian sediments have been linked to hydrothermal inputs (Yang et al., 2008). For these reasons, we do not consider P and Ba in the discussion of paleoproductivity for the Yuanjia section.

### 6.4. Possible mechanisms for super-heavy $\delta^{238}U$ values

Given a seawater $\delta^{238}U$ of −0.65‰ to −0.45‰ in the early Cambrian (Dahl et al., 2017), 14 out of 27 samples at Yuanjia show super-heavy $\delta^{238}U$ values (i.e., > +0.15‰) that are inconsistent with a porewater fractionation mechanism (see Section 5.3; Figs. 2 and 3). Similar super-heavy U isotopic compositions have previously been reported only from a handful of ancient marine units, e.g., Unit II of the Black Sea (Montoya-Pino et al., 2010) and Member IV of the Doushantuo Formation (Kendall et al., 2015). Andersen et al. (2014) proposed that partial U removal under suboxic bottom-water environment can cause isotope fractionation larger than +0.6‰. However, this mechanism cannot explain the super-heavy $\delta^{238}U$ values observed at Yuanjia because: (1) the study black shales deposited under persistently euxinic conditions rather than suboxic conditions (see Section 5.1), and (2) the partial U removal causes limited U accumulation in the sediment, inconsistent with the generally high enrichments of U at Yuanjia (Fig. 2).

Organic matter may have played an important role in authigenic U accumulation and isotopic fractionation in the organic-rich Yuanjia shales. This is indicated *inter alia* by a strong positive correlation between U concentrations and TOC ($R^2 = 0.63$, $p < 0.05$; Fig. 6D). As in modern highly productive regions such as the California Margin, U reduction and uptake by organic particles can account

Please cite this article in press as: Cheng M., et al. Evidence for high organic carbon export to the early Cambrian seafloor. *Geochim. Cosmochim. Acta* (2020), https://doi.org/10.1016/j.gca.2020.01.050

for the bulk of the U burial flux (Zheng et al., 2002; McManus et al., 2005). Holmden et al. (2015) reported a negative isotope fractionation of $-0.79 \pm 0.17$‰ associated with U adsorption to plankton. If universal, then sedimentary organic-hosted U should generally exhibit low $\delta^{238}U$ values, which, however, does not accord with the super-heavy $\delta^{238}U$ values observed at Yuanjia. Therefore, U adsorption by organic matter cannot explain the super-heavy $\delta^{238}U$ values at Yuanjia.

We propose that the super-heavy $\delta^{238}U$ values observed at Yuanjia may have been a product of U reduction within a high-porosity sediment layer on the seafloor, i.e., a benthic organic flocculent layer. Such flocculent layers tend to develop at the sediment–water interface under conditions of high productivity and low benthic faunal activity (e.g., due to anoxic bottomwater conditions). They are generally characterized with ~2 cm in thickness, mottled gray-black/gray-green in color and a jelly-like consistency, and with high concentrations of bacteria on the surface or within (İzdar and Murray, 1989). In this high-porosity layer, U (VI) can be reduced to U(IV), and the accompanying isotopic fractionation is not (or slightly if any) limited by the transport-diffusion process as in porewaters and thus can yield $\Delta^{238}U$ values close to the theoretical maximum fractionation of ~+1.2‰ (cf. Andersen et al., 2017; their Fig. 7a). A near-modern analog is Holocene Black Sea Unit II, which was formed under a flocculent layer (İzdar and Murray, 1989), a sapropel with up to 15% TOC (Arthur and Dean, 1998) and $\delta^{238}U$ as high as +0.43‰ (Montoya-Pino et al., 2010). This unit recorded high productivity during the transition of Black Sea from an oxic, freshwater lake to an anoxic, saline basin at ~7.5 ka (Arthur and Dean, 1998). At Yuanjia, samples with super-heavy $\delta^{238}U$ values are enriched in the nutrient elements Cu, Zn, Ni and Cd (Figs. 3 and 7), which is also observed in Unit II of Black Sea (Piper and Calvert, 2011), supporting the inference that the U reduction process was related to high productivity. Another modern analog is Mono Lake in eastern California, USA, which holds alkaline, euxinic water condition and yields U isotope fractionation of ~1.1‰ between the lake water and sediment (Jemison et al., 2018). This large fractionation has been also explained as a result of U reduction in the water column (Jemison et al., 2018), although we don't know whether a flocculent layer develops there.

In benthic flocculent layers, U reduction is catalyzed by the activity of sulfate-reducing bacteria and/or presence of $H_2S$, variations of which may influence U reduction rates. Based on laboratory experiments, Stylo et al. (2015) argued that microbial reduction of U(VI) is readily distinguishable from abiotic U(VI) reduction because U isotope fractionation is associated only with the former process. However, Brown et al. (2018) showed that abiotic U isotope fractionation can occur in any reduced environment. Our U isotope data cannot tell the U reduction at Yuanjia is a biotic or abiotic process. The magnitude of isotopic fractionation during U reduction is also thought to increase at slower aqueous U removal rates and, thus, at lower [$H_2S$] or weaker activity of sulfate reduction bacteria (which actually should result in lower [$H_2S$]) (Brown et al., 2018). $\delta^{98}Mo$ values at Yuanjia were controlled by local sulfidity levels (Section 6.2), providing an independent means of evaluating this watermass parameter. Lower $\delta^{98}Mo$ corresponds to lower [$H_2S$], and, thus, presumably also to lower U removal rates and higher $\delta^{238}U$ values. These relationships are indeed supported by the strong negative correlation between $\delta^{238}U$ and $\delta^{98}Mo$ at Yuanjia ($R^2 = 0.40$; $p = 0.03$; Fig. 6A). Although these relationships do not directly prove the existence of a benthic organic flocculent layer on the Yuanjia seafloor, they are well consistent with the existence of such a layer, which would have been readily formed in a euxinic deepwater setting under conditions of high surface-water productivity.

### 6.5. Oceanic upwelling as a trigger for the formation of benthic organic flocculent layer

Significant covariation of $\delta^{98}Mo$, $\delta^{238}U$ and nutrient elements (Cu, Zn, Ni and Cd) (Figs. 3, 6A, 7) indicates that changes in watermass sulfidity (Section 6.2), U reduction rates (Section 6.4), and primary productivity (Section 6.3) must have occurred concurrently at Yuanjia. As shown by sapropel S5 of the Black Sea (Andersen et al., 2018), bottom-water $H_2S$ concentrations are significantly influenced by deep-water renewal rate. Similarly, in the modern ocean, variations of local marine nutrient fluxes and productivity are mainly caused by varying patterns of seawater circulation and their influence on upwelling rates, which control nutrient fluxes from deep waters to the euphotic zone (Schoepfer et al., 2015). Widespread occurrence of phosphorite deposits in the lower Cambrian Niutitang Formation and stratigraphic equivalents globally have been widely attributed to coeval strong deep-water upwelling (Meert and Lieberman, 2008; Papineau, 2010; Yeasmin et al., 2017; Gao et al., 2018; Xiang et al., 2018; Jin et al., 2020). Therefore, it is reasonable to infer that variations in upwelling intensity or rates of deepwater renewal controlled both productivity and bottom-water $H_2S$ concentrations in the early Cambrian Nanhua Basin.

We propose that the formation of benthic organic flocculent layer at Yuanjia was related to episodic upwelling events from the open ocean, which provided higher nutrient fluxes for primary producers, resulting in enhanced productivity (Fig. 8). With enhanced primary productivity, organic matter produced in the surface waters settled through the water column and accumulated on the seafloor to form the flocculent layer, within which U was reduced with a large positive isotopic fractionation (see Section 6.4) and subsequently buried (Fig. 8A). Owing to low oxygen and sulfate levels in early Cambrian seawater (Sperling et al., 2015b; Jin et al., 2016), intensified upwelling would have led to deep-water renewal and inhibited the buildup of $H_2S$, leading to lower [$H_2S$] and, in turn, lower $\delta^{98}Mo$ values in the sediment (Fig. 8B). In contrast, without intensified upwelling, the transfer efficiency of nutrient elements from the deep ocean to the euphotic zone would be weakened, resulting in lower productivity, weaker organic export, limited accumulation of organic floccules, more U reduction in sedimentary porewaters and, thus, lower $\delta^{238}U$ (Fig. 8C). During such episodes, limited deepwater

Please cite this article in press as: Cheng M., et al. Evidence for high organic carbon export to the early Cambrian seafloor. *Geochim. Cosmochim. Acta* (2020), https://doi.org/10.1016/j.gca.2020.01.050

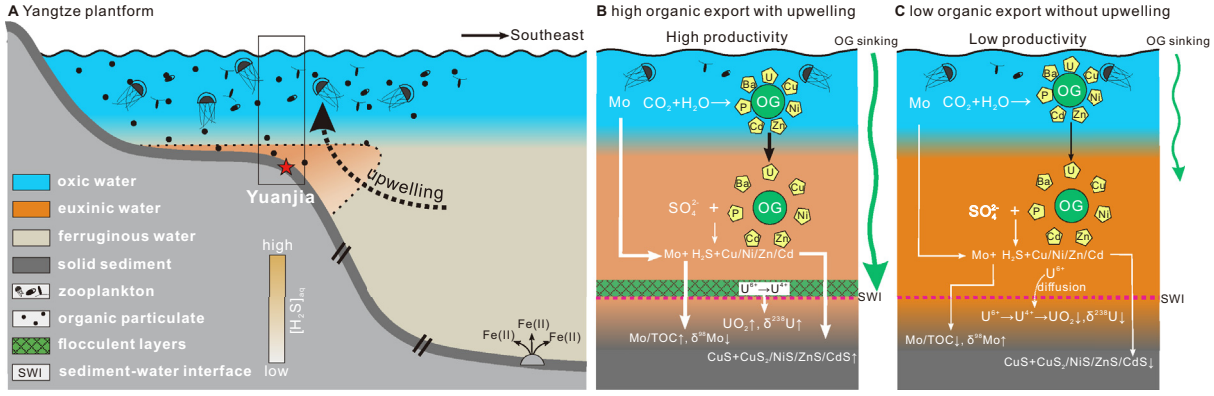


Fig. 8. Conceptual model for the seafloor flocculent layer formation in early Cambrian Nanhua Basin. (A) Yangtze Platform; (B) strong upwelling, leading to enhanced organic export, seafloor flocculent layer formation, high $\delta^{238}U$ values, high nutrient metal enrichments, rapid deep-water renewal, low $[H_2S]_{aq}$, and low $\delta^{98}Mo$ in the sediment; (C) weak upwelling, leading to inverse effects and geochemical patterns to those cited for (B). See text for more details.

renewal allowed $[H_2S]$ to build up, as reflected in higher $\delta^{98}Mo$ values.

In the modern ocean, wind-driven upwelling, as on the California/Oregon/Washington margins in the North Pacific, the Peru and Chile margins in the South Pacific, the Northwest Africa and Portugal margins in the North Atlantic, and the South Africa/Namibia margins in the South Atlantic, always causes higher productivity, expansion of oxygen-minimum zones (OMZs), and enhanced organic carbon burial (Kämpf and Chapman, 2016), but corresponding development of benthic organic flocculent layers was not reported. In addition, although U isotope data from these regions are still rare, no super-heavy $\delta^{238}U$ values have been reported (e.g., Abshire et al., 2020). This may likely indicate that upwelling itself is not sufficient for the development of such flocculent layer in early Cambrian oceans. The early Cambrian oceans might have higher background of nutrient availability due to the strong continental weathering as indicated by the high $^{87}Sr/^{86}Sr$ ratios (Maloof et al., 2010). As observed at Yuanjia and many other contemporaneous sections with different water depths, euxinia prevalently developed on the continental shelf (e.g., Feng et al., 2014; Sperling et al., 2015b; Jin et al., 2016; Li et al., 2017), the toxic $H_2S$ will kill any benthic animals in these areas. Additionally, the deposition of black shales always occurs in environment with little to no bottom currents. Under these unique conditions, organic matters produced in the euphotic zone of the Cambrian ocean might be greater in amount than modern upwelling areas and sink through the water column and accumulated on the sediment-water interface easier, without being decomposed by oxygen or animals, forming a flocculent layer on the seafloor.

### 6.6. High organic carbon export fluxes in early Cambrian oceans and implications for the atmospheric-oceanic oxygenation and Cambrian Explosion

Our Fe-U-Mo-Cu-Zn-Ni-Cd systematic data at Yuanjia supports the episodic developments of benthic organic flocculent layer triggered by marine upwellings in the early Cambrian Nanhua Basin, which provide direct evidence for high fluxes of organic matter to the sediment in the early Cambrian oceans. This inference is consistent with the extremely high organic carbon accumulation rates (OCAR) at Yuanjia which are between 2600 and 14,000 mg $cm^{-2}$ $kyr^{-1}$ with a mean of 5,600 mg $cm^{-2}$ $kyr^{-1}$ for Yuanjia. These values are higher than OCAR in most modern oceanic sediments, e.g., the oxic Equatorial Pacific Ocean (14 ± 11 mg $cm^{-2}$ $kyr^{-1}$), anoxic Black Sea (217 ± 243 mg $cm^{-2}$ $kyr^{-1}$), and high-productivity Peru Margin (369 ± 384 mg $cm^{-2}$ $kyr^{-1}$), but similar to Saanich Inlet (8,768 ± 2,258 mg $cm^{-2}$ $kyr^{-1}$) (Schoepfer et al., 2015), which is a weakly euxinic basin with high sedimentation rates (Algeo and Lyons, 2006). These values are indicative of elevated organic carbon burial rates in the early Cambrian ocean of the South China Craton. Given the global prevalence of lower Cambrian organic-rich black shales (Condie et al., 2001), the observations above at Yuanjia may have been typical of early Cambrian oceans, representing a major organic carbon export and in turn burial event in the early Cambrian oceans.

Enhanced burial of organic carbon is likely to have caused a net decrease in $CO_2$ and a net increase in $O_2$ in the early Cambrian ocean-atmosphere system. A decrease in atmospheric $CO_2$ would have led to a climatic cooling trend, which is consistent with evidence of mid-Cambrian continental glaciation (Landing and MacGabhann, 2010). Organic carbon burial also would have released large amounts of $O_2$ to the atmosphere (Lenton et al., 2014; Daines et al., 2017), driving expansion of the oxic ocean-surface layer and promoting metazoan diversification and ecological expansion (Sperling et al., 2015b; Cheng et al., 2017; Li et al., 2017; Li et al., 2018; Wang et al., 2018; Dahl et al., 2019). Rising oxygen levels may have likely generated a positive feedback through animal evolution during the Cambrian, as increases in diversity and biomass led to further enhancement of organic matter export and burial (Logan et al., 1995; Lenton et al., 2014; Li et al., 2018). This feedback would have operated until rising oxygen levels increased rates of organic matter oxidation sufficiently to establish a new biogeochemical equilibrium, a point potentially marked by the shift from black shale to carbonate sedimentation on most continents during early Cambrian

Please cite this article in press as: Cheng M., et al. Evidence for high organic carbon export to the early Cambrian seafloor. *Geochim. Cosmochim. Acta* (2020), https://doi.org/10.1016/j.gca.2020.01.050

Stage 3 (Zhu et al., 2003). Taken together, our study supports the hypothesis that enhanced organic burial triggered a major atmospheric-oceanic oxygenation event that stimulated the subsequent explosion of Cambrian life, thus providing a key link between the contemporaneous atmospheric and oceanic oxygenation and bioevolutionary events although these processes could also interact potentially.

## 7. CONCLUSIONS

In order to test the hypothesis that high organic export and burial triggered the rise of oxygen levels in the contemporaneous atmosphere-ocean system and the Cambrian Explosion, an integrated analysis of U isotopes, Mo isotopes, iron speciation, major and trace elements was conducted for the lower Cambrian organic-rich black shales of the Yuanjia section in South China. Our iron speciation ratios and Mo-U enrichment data indicate that local redox conditions at Yuanjia were persistently euxinic but the large range of $\delta^{98}$Mo indicates variable $H_2S$ concentrations lower than the threshold value (~11 μm) for quantitative Mo precipitation. Mo-U relationships indicate that the early Cambrian Nanhua Basin was connected to the open ocean although its partial restriction cannot be precluded. Nutrient-element (Cu, Zn, Ni and Cd) enrichments suggest a high and variable primary and export productivity at Yuanjia. Most importantly, more than half of the Yuanjia black shales exhibit "super heavy" $\delta^{238}$U values (to +0.84‰) that cannot be explained by normal pore-water U-isotopic fractionation mechanism, and suggest U reduction most likely within a benthic organic flocculent layer on the seafloor, where U isotope fractionation can be much larger than in sediment porewaters. Based on the strong covariation of $\delta^{98}$Mo, $\delta^{238}$U and nutrient elements (Cu, Zn, Ni and Cd) and all information collected above, we propose that the formation of benthic organic flocculent layer at Yuanjia was related to episodic upwelling events from open ocean. The episodic developments of benthic organic flocculent layer and high primary productivity in the early Cambrian Nanhua Basin as inferred by our Fe-U-Mo-Cu-Zn-Ni-Cd systematic data at Yuanjia, along with high organic carbon accumulation rates (mean: 5600 mg cm$^{-2}$ kyr$^{-1}$), provide direct evidence for high fluxes of organic matter to the sediment in the early Cambrian oceans, providing a key link between the Cambrian Explosion and the contemporaneous atmospheric and oceanic oxygenation through high organic burial.

## Declaration of Competing Interest

The authors declare that they have no known competing financial interests or personal relationships that could have appeared to influence the work reported in this paper.

## ACKNOWLEDGMENTS

We thank Shi-Da Tang, Gwyneth W. Gordon and Stephen Romaniello for their field and laboratory assistance and helpful discussions. This study was funded by Strategic Priority Research Program of Chinese Academy of Sciences (Grant # XDB26000000), NSFC (Grants # 41825019, 41703008, 41821001, 41902027), the National Key R&D Program of China (Grant # 2016YFA0601100), and NSFC-RCUK_NERC Program (Grant # 41661134048). TWL acknowledges support from the NASA Astrobiology Institute Alternative Earths team under Cooperative Agreement Number NNA15BB03A. TJA acknowledges support from the Sedimentary Geology and Paleobiology program of NSF (Grant # EAR-1733977).

## APPENDIX A. SUPPLEMENTARY MATERIAL

Supplementary data to this article can be found online at https://doi.org/10.1016/j.gca.2020.01.050.

## REFERENCES

Abe M., Suzuki T., Fujii Y., Hada M. and Hirao K. (2008) An ab initio molecular orbital study of the nuclear volume effects in uranium isotope fractionations. *J. Chem. Phys.* **129** 164309.

Abshire M. L., Romaniello S. J., Kuzminov A. M., Cofrancesco J., Severmann S. and Riedinger N. (2020) Uranium isotopes as a proxy for primary depositional redox conditions in organic-rich marine systems. *Earth. Planet. Sci. Lett.* **529** 115878.

Algeo T. J., Henderson C. M., Tong J., Feng Q., Yin H. and Tyson R. V. (2013) Plankton and productivity during the Permian-Triassic boundary crisis: an analysis of organic carbon fluxes. *Global Planet Change* **105**, 52–67.

Algeo T. J. and Lyons T. W. (2006) Mo-total organic carbon covariation in modern anoxic marine environments: Implications for analysis of paleoredox and paleohydrographic conditions. *Paleoceanography* **21**. https://doi.org/10.1029/2004pa001112.

Algeo T. J. and Maynard J. B. (2004) Trace-element behavior and redox facies in core shales of Upper Pennsylvanian Kansas-type cyclothems. *Chem. Geol.* **206**, 289–318.

Algeo T. J. and Tribovillard N. (2009) Environmental analysis of paleoceanographic systems based on molybdenum–uranium covariation. *Chem. Geol.* **268**, 211–225.

Anbar A. D., Knab K. A. and Barling J. (2001) Precise determination of mass-dependent variations in the isotopic composition of molybdenum using MC-ICPMS. *Anal. Chem.* **73**, 1425–1431.

Andersen M. B., Matthews A., Vance D., Bar-Matthews M., Archer C. and de Souza G. F. (2018) A 10-fold decline in the deep Eastern Mediterranean thermohaline overturning circulation during the last interglacial period. *Earth. Planet. Sci. Lett.* **503**, 58–67.

Andersen M. B., Romaniello S., Vance D., Little S. H., Herdman R. and Lyons T. W. (2014) A modern framework for the interpretation of $^{238}$U/$^{235}$U in studies of ancient ocean redox. *Earth. Planet. Sci. Lett.* **400**, 184–194.

Andersen M. B., Stirling C. H. and Weyer S. (2017) Uranium isotope fractionation. *Rev. Mineral. Geochem.* **82**, 799–850.

Anderson R., LeHuray A., Fleisher M. and Murray J. (1989) Uranium deposition in Saanich Inlet sediments, Vancouver Island. *Geochim. Cosmochim. Acta* **53**, 2205–2213.

Archer C. and Vance D. (2008) The isotopic signature of the global riverine molybdenum flux and anoxia in the ancient oceans. *Nat. Geosci.* **1**, 597–600.

Arnold G. L., Anbar A. D., Barling J. and Lyons T. W. (2004) Molybdenum isotope evidence for widespread anoxia in mid-Proterozoic oceans. *Science* **304**, 87–90.

Arthur M. A. and Dean W. E. (1998) Organic-matter production and preservation and evolution of anoxia in the Holocene Black Sea. *Paleoceanography* **13**, 395–411.

Barling J. and Anbar A. D. (2004) Molybdenum isotope fractionation during adsorption by manganese oxides. *Earth. Planet. Sci. Lett.* **217**, 315–329.

Basu A., Sanford R. A., Johnson T. M., Lundstrom C. C. and Löffler F. E. (2014) Uranium isotopic fractionation factors during U(VI) reduction by bacterial isolates. *Geochim. Cosmochim. Acta* **136**, 100–113.

Bigeleisen J. (1996) Nuclear size and shape effects in chemical reactions. Isotope chemistry of the heavy elements. *J. Amer. Chem. Soci.* **118**, 3676–3680.

Böning P., Brumsack H.-J., Böttcher M. E., Schnetger B., Kriete C., Kallmeyer J. and Borchers S. L. (2004) Geochemistry of Peruvian near-surface sediments. *Geochim. Cosmochim. Acta* **68**, 4429–4451.

Boyd P. W., Ellwood M. J., Tagliabue A. and Twining B. S. (2017) Biotic and abiotic retention, recycling and remineralization of metals in the ocean. *Nat. Geosci.* **10**, 167–173.

Breitburg D., Levin L. A., Oschlies A., Gregoire M., Chavez F. P., Conley D. J., Garcon V., Gilbert D., Gutierrez D., Isensee K., Jacinto G. S., Limburg K. E., Montes I., Naqvi S. W. A., Pitcher G. C., Rabalais N. N., Roman M. R., Rose K. A., Seibel B. A., Telszewski M., Yasuhara M. and Zhang J. (2018) Declining oxygen in the global ocean and coastal waters. *Science* **359**.

Brennecka G. A., Herrmann A. D., Algeo T. J. and Anbar A. D. (2011a) Rapid expansion of oceanic anoxia immediately before the end-Permian mass extinction. *Proc. Natl. Acad. Sci. U. S. A.* **108**, 17631–17634.

Brennecka G. A., Wasylenki L. E., Bargar J. R., Weyer S. and Anbar A. D. (2011b) Uranium isotope fractionation during adsorption to Mn-oxyhydroxides. *Environ. Sci. Technol.* **45**, 1370–1375.

Brocks J. J., Jarrett A. J. M., Sirantoine E., Hallmann C., Hoshino Y. and Liyanage T. (2017) The rise of algae in Cryogenian oceans and the emergence of animals. *Nature* **548**, 578–581.

Brown S. T., Basu A., Ding X., Christensen J. N. and DePaolo D. J. (2018) Uranium isotope fractionation by abiotic reductive precipitation. *Proc. Natl. Acad. Sci. U. S. A.* **115**, 8688–8693.

Bura-Nakić E., Andersen M. B., Archer C., de Souza G. F., Marguš M. and Vance D. (2018) Coupled Mo-U abundances and isotopes in a small marine euxinic basin: constraints on processes in euxinic basins. *Geochim. Cosmochim. Acta* **222**, 212–229.

Chen D., Zhou X., Fu Y., Wang J. and Yan D. (2015a) New U-Pb zircon ages of the Ediacaran-Cambrian boundary strata in South China. *Terra Nova* **27**, 62–68.

Chen X., Ling H. F., Vance D., Shields-Zhou G. A., Zhu M., Poulton S. W., Och L. M., Jiang S. Y., Li D., Cremonese L. and Archer C. (2015b) Rise to modern levels of ocean oxygenation coincided with the Cambrian radiation of animals. *Nat. Commun.* **6**, 7.

Chen X. M., Romaniello S. J., Herrmann A. D., Samankassou E. and Anbar A. D. (2018) Biological effects on uranium isotope fractionation ($^{238}U/^{235}U$) in primary biogeneic carbonates. *Geochim. Cosmochim. Acta* **240**, 1–10.

Cheng M., Li C., Zhou L., Algeo T. J., Zhang F., Romaniello S., Jin C.-S., Lei L.-D., Feng L.-J. and Jiang S.-Y. (2016) Marine Mo biogeochemistry in the context of dynamically euxinic mid-depth waters: a case study of the lower Cambrian Niutitang shales, South China. *Geochim. Cosmochim. Acta* **183**, 79–93.

Cheng M., Li C., Zhou L., Feng L., Algeo T. J., Zhang F., Romaniello S., Jin C., Ling H. and Jiang S. (2017) Transient deep-water oxygenation in the early Cambrian Nanhua Basin, South China. *Geochim. Cosmochim. Acta* **210**, 42–58.

Clarkson M. O., Poulton S. W., Guilbaud R. and Wood R. A. (2014) Assessing the utility of Fe/Al and Fe-speciation to record water column redox conditions in carbonate-rich sediments. *Chem. Geol.* **382**, 111–122.

Condie K. C., Marais D. J. D. and Abbott D. (2001) Precambrian superplumes and supercontinents: a record in black shales, carbon isotopes, and paleoclimates? *Precambr. Res.* **106**, 239–260.

Dahl T. W., Connelly J. N., Kouchinsky A., Gill B. C., Månsson S. F. and Bizzarro M. (2017) Reorganisation of Earth's biogeochemical cycles briefly oxygenated the oceans 520 Myr ago. *Geochem. Perspect. Lett.* **3**, 210–220.

Dahl T. W., Connelly J. N., Li D., Kouchinsky A., Gill B. C., Porter S., Maloof A. C. and Bizzarro M. (2019) Atmosphere-ocean oxygen and productivity dynamics during early animal radiations. *Proc. Natl. Acad. Sci. U. S. A.* **116**, 19352–19361.

Dahl T. W., Hammarlund E. U., Anbar A. D., Bond D. P. G., Gill B. C., Gordon G. W., Knoll A. H., Nielsen A. T., Schovsbo N. H. and Canfield D. E. (2010) Devonian rise in atmospheric oxygen correlated to the radiations of terrestrial plants and large predatory fish. *Proc. Natl. Acad. Sci. U. S. A.* **107**, 17911–17915.

Daines S. J., Mills B. J. and Lenton T. M. (2017) Atmospheric oxygen regulation at low Proterozoic levels by incomplete oxidative weathering of sedimentary organic carbon. *Nat. Commun.* **8**, 14379.

Dickson A. J. (2017) A molybdenum-isotope perspective on Phanerozoic deoxygenation events. *Nat. Geosci.* **10**, 721–726.

Dickson A. J., Cohen A. S. and Coe A. L. (2014) Continental margin molybdenum isotope signatures from the early Eocene. *Earth. Planet. Sci. Lett.* **404**, 389–395.

Erickson B. E. and Helz G. R. (2000) Molybdenum(VI) speciation in sulfidic waters: stabiloty and lability of thiomolybdates. *Geochim. Cosmochim. Acta* **64**, 1149–1158.

Erwin D. H., Laflamme M., Tweedt S. M., Sperling E. A., Pisani D. and Peterson K. J. (2011) The Cambrian conundrum: early divergence and later ecological success in the early history of animals. *Science* **334**, 1091–1097.

Feng L., Li C., Huang J., Chang H. and Chu X. (2014) A sulfate control on marine mid-depth euxinia on the early Cambrian (ca. 529–521 Ma) Yangtze platform, South China. *Precambr. Res.* **246**, 123–133.

Gao P., He Z., Li S., Lash G. G., Li B., Huang B. and Yan D. (2018) Volcanic and hydrothermal activities recorded in phosphate nodules from the Lower Cambrian Niutitang Formation black shales in South China. *Palaeogeogr. Palaeoclimatol. Palaeoecol.* **505**, 381–397.

Gardner C. B., Carey A. E., Lyons W. B., Goldsmith S. T., McAdams B. C. and Trierweiler A. M. (2017) Molybdenum, vanadium, and uranium weathering in small mountainous rivers and rivers draining high-standing islands. *Geochim. Cosmochim. Acta* **219**, 22–43.

Goldberg T., Archer C., Vance D. and Poulton S. W. (2009) Mo isotope fractionation during adsorption to Fe (oxyhydr)oxides. *Geochim. Cosmochim. Acta* **73**, 6502–6516.

Goldberg T., Gordon G., Izon G., Archer C., Pearce C. R., McManus J., Anbar A. D. and Rehkämper M. (2013) Resolution of inter-laboratory discrepancies in Mo isotope data: an intercalibration. *J. Annal. Atom. Spectrom.* **28**, 724–735.

Goto K. T., Anbar A. D., Gordon G. W., Romaniello S. J., Shimoda G., Takaya Y., Tokumaru A., Nozaki T., Suzuki K., Machida S., Hanyu T. and Usui A. (2014) Uranium isotope systematics of ferromanganese crusts in the Pacific Ocean:

implications for the marine $^{238}U/^{235}U$ isotope system. *Geochim. Cosmochim. Acta* **146**, 43–58.

Guo Q., Strauss H., Zhu M., Zhang J., Yang X., Lu M. and Zhao F. (2013) High resolution organic carbon isotope stratigraphy from a slope to basinal setting on the Yangtze Platform, South China: implications for the Ediacaran-Cambrian transition. *Precambr. Res.* **225**, 209–217.

Hinojosa J. L., Stirling C. H., Reid M. R., Moy C. M. and Wilson G. S. (2016) Trace metal cycling and $^{238}U/^{235}U$ in New Zealand's fjords: implications for reconstructing global paleo-redox conditions in organic-rich sediments. *Geochim. Cosmochim. Acta* **179**, 89–109.

Holmden C., Amini M. and Francois R. (2015) Uranium isotope fractionation in Saanich Inlet: a modern analog study of a paleoredox tracer. *Geochim. Cosmochim. Acta* **153**, 202–215.

İzdar E. and Murray J. W. (1989) *Black Sea Oceanography*. Springer Science & Business Media.

Jemison N., Brown S. and Druhan J. (2018) Large $^{238}U$–$^{235}U$ fractionation in an alkaline, euxinic lake: implications for the marine sedimentary record. *Goldschmidt* **20**, 18.

Jemison N. E., Johnson T. M., Shiel A. E. and Lundstrom C. C. (2016) Uranium isotopic fractionation induced by U(VI) adsorption onto common aquifer minerals. *Environ. Sci. Technol.* **50**, 12232–12240.

Jin C., Li C., Algeo T. J., Planavsky N. J., Cui H., Yang X., Zhao Y., Zhang X. and Xie S. (2016) A highly redox-heterogeneous ocean in South China during the early Cambrian (~529–514 Ma): Implications for biota-environment co-evolution. *Earth. Planet. Sci. Lett.* **441**, 38–51.

Jin C., Li C., Algeo T. J., Wu S., Cheng M., Zhang Z. and Shi W. (2020) Controls on organic matter accumulation on the early-Cambrian western Yangtze Platform, South China. *Mari. Petrol. Geol.* **111**, 75–87.

Kämpf J. and Chapman P. (2016) *Upwelling Systems of the World*. Springer International Publishing, Switzerland.

Kendall B., Brennecka G. A., Weyer S. and Anbar A. D. (2013) Uranium isotope fractionation suggests oxidative uranium mobilization at 2.50 Ga. *Chem. Geol.* **362**, 105–114.

Kendall B., Dahl T. W. and Anbar A. D. (2017) The stable isotope geochemistry of molybdenum. *Rev. Mineral. Geochem.* **82**, 683–732.

Kendall B., Komiya T., Lyons T. W., Bates S. M., Gordon G. W., Romaniello S. J., Jiang G. Q., Creaser R. A., Xiao S. H., McFadden K., Sawaki Y., Tahata M., Shu D. G., Han J., Li Y., Chu X. L. and Anbar A. D. (2015) Uranium and molybdenum isotope evidence for an episode of widespread ocean oxygenation during the late Ediacaran Period. *Geochim. Cosmochim. Acta* **156**, 173–193.

King E. K., Perakis S. S. and Pett-Ridge J. C. (2018) Molybdenum isotope fractionation during adsorption to organic matter. *Geochim. Cosmochim. Acta* **222**, 584–598.

Landing E. and MacGabhann B. A. (2010) First evidence for Cambrian glaciation provided by sections in Avalonian New Brunswick and Ireland: additional data for Avalon-Gondwana separation by the earliest Palaeozoic. *Palaeogeogr. Palaeoclimatol. Palaeoecol.* **285**, 174–185.

Large R. R., Halpin J. A., Danyushevsky L. V., Maslennikov V. V., Bull S. W., Long J. A., Gregory D. D., Lounejeva E., Lyons T. W., Sack P. J., McGoldrick P. J. and Calver C. R. (2014) Trace element content of sedimentary pyrite as a new proxy for deep-time ocean–atmosphere evolution. *Earth. Planet. Sci. Lett.* **389**, 209–220.

Lenton T. M., Boyle R. A., Poulton S. W., Shields-Zhou G. A. and Butterfield N. J. (2014) Co-evolution of eukaryotes and ocean oxygenation in the Neoproterozoic era. *Nat. Geosci.* **7**, 257–265.

Li C., Cheng M., Zhu M. and Lyons T. W. (2018) Heterogeneous and dynamic marine shelf oxygenation and coupled early animal evolution. *Emerg. Top. Life Sci.* **2**, 279–288.

Li C., Jin C., Planavsky N. J., Algeo T. J., Cheng M., Yang X., Zhao Y. and Xie S. (2017) Coupled oceanic oxygenation and metazoan diversification during the early–middle Cambrian? *Geology* **45**, 743–746.

Li C., Planavsky N. J., Shi W., Zhang Z., Zhou C., Cheng M., Tarhan L. G., Luo G. and Xie S. (2015) Ediacaran marine redox heterogeneity and early animal ecosystems. *Sci. Rep.* **5**, 8 pp.

Logan G. A., Hayes J. M., Hieshima G. B. and Summons R. E. (1995) Terminal Proterozoic reorganization of biogeochemical cycles. *Nature* **376**, 53–56.

Lu X., Kendall B., Stein H. J., Li C., Hannah J. L., Gordon G. W. and Ebbestad J. O. R. (2017) Marine redox conditions during deposition of Late Ordovician and Early Silurian organic-rich mudrocks in the Siljan ring district, central Sweden. *Chem. Geol.* **457**, 75–94.

Maloof A. C., Porter S. M., Moore J. L., Dudas F. O., Bowring S. A., Higgins J. A., Fike D. A. and Eddy M. P. (2010) The earliest Cambrian record of animals and ocean geochemical change. *Geol. Soc. Am. Bull.* **122**, 1731–1774.

McLennan S. M. (2001) Relationships between the trace element composition of sedimentary rocks and upper continental crust. *Geochem. Geophys. Geosyst.* **2**. https://doi.org/10.1029/2000GC000109.

McManus J., Berelson W. M., Klinkhammer G. P., Hammond D. E. and Holm C. (2005) Authigenic uranium: Relationship to oxygen penetration depth and organic carbon rain. *Geochim. Cosmochim. Acta* **69**, 95–108.

Meert J. G. and Lieberman B. S. (2008) The Neoproterozoic assembly of Gondwana and its relationship to the Ediacaran-Cambrian radiation. *Gondwana Res.* **14**, 5–21.

Montoya-Pino C., Weyer S., Anbar A. D., Pross J., Oschmann W., van de Schootbrugge B. and Arz H. W. (2010) Global enhancement of ocean anoxia during Oceanic Anoxic Event 2: a quantitative approach using U isotopes. *Geology* **38**, 315–318.

Morford J. L. and Emerson S. (1999) The geochemistry of redox sensitive trace metals in sediments. *Geochim. Cosmochim. Acta* **63**, 1735–1750.

Nakagawa Y., Takano S., Firdaus M. L., Norisuye K., Hirata T., Vance D. and Sohrin Y. (2012) The molybdenum isotopic composition of the modern ocean. *Geochem. J.* **46**, 131–141.

Nägler T. F., Anbar A. D., Archer C., Goldberg T., Gordon G. W., Greber N. D., Siebert C., Sohrin Y. and Vance D. (2013) Proposal for an international molybdenum isotope measurement standard and data representation. *Geostand. Geoanal. Res.* **38**, 149–151.

Neubert N., Nägler T. F. and Böttcher M. E. (2008) Sulfidity controls molybdenum isotope fractionation into euxinic sediments: evidence from the modern Black Sea. *Geology* **36**, 775–778.

Noordmann J., Weyer S., Montoya-Pino C., Dellwig O., Neubert N., Eckert S., Paetzel M. and Böttcher M. E. (2015) Uranium and molybdenum isotope systematics in modern euxinic basins: case studies from the central Baltic Sea and the Kyllaren fjord (Norway). *Chem. Geol.* **396**, 182–195.

Och L. M. and Shields-Zhou G. A. (2012) The Neoproterozoic oxygenation event: environmental perturbations and biogeochemical cycling. *Earth-Sci Rev* **110**, 26–57.

Papineau D. (2010) Global biologeochemical changes at both ends of the proterozoic: insights from phosphorites. *Astrobiology* **10**, 165–181.

Please cite this article in press as: Cheng M., et al. Evidence for high organic carbon export to the early Cambrian seafloor. *Geochim. Cosmochim. Acta* (2020), https://doi.org/10.1016/j.gca.2020.01.050

Piper D. Z. and Calvert S. E. (2011) Holocene and late glacial palaeoceanography and palaeolimnology of the Black Sea: changing sediment provenance and basin hydrography over the past 20,000years. *Geochim. Cosmochim. Acta* **75**, 5597–5624.

Poulson R. L., Siebert C., McManus J. and Berelson W. M. (2006) Authigenic molybdenum isotope signatures in marine sediments. *Geology* **34**, 617–620.

Poulton S. and Canfield D. (2005) Development of a sequential extraction procedure for iron: implications for iron partitioning in continentally derived particulates. *Chem. Geol.* **214**, 209–221.

Poulton S. W. and Canfield D. E. (2011) Ferruginous conditions: a dominant feature of the ocean through Earth's history. *Elements* **7**, 107–112.

Rolison J. M., Stirling C. H., Middag R. and Rijkenberg M. J. A. (2017) Uranium stable isotope fractionation in the Black Sea: modern calibration of the $^{238}U/^{235}U$ paleo-redox proxy. *Geochim. Cosmochim. Acta* **203**, 69–88.

Romaniello S. J., Herrmann A. D. and Anbar A. D. (2013) Uranium concentrations and $^{238}U/^{235}U$ isotope ratios in modern carbonates from the Bahamas: assessing a novel paleoredox proxy. *Chem. Geol.* **362**, 305–316.

Schoepfer S. D., Shen J., Wei H., Tyson R. V., Ingall E. and Algeo T. J. (2015) Total organic carbon, organic phosphorus, and biogenic barium fluxes as proxies for paleomarine productivity. *Earth-Sci. Rev.* **149**, 23–52.

Shi W., Li C., Luo G., Huang J., Algeo T. J., Jin C., Zhang Z. and Cheng M. (2018) Sulfur isotope evidence for transient marine-shelf oxidation during the Ediacaran Shuram Excursion. *Geology* **46**, 267–270.

Shu D. (2008) Cambrian explosion: birth of tree of animals. *Gondwana Res.* **14**, 219–240.

Sperling E. A., Knoll A. H. and Girguis P. R. (2015a) The ecological physiology of earth's second oxygen revolution. *Ann. Rev. Ecol., Evolut., Systemat.* **46**, 215–235.

Sperling E. A., Wolock C. J., Morgan A. S., Gill B. C., Kunzmann M., Halverson G. P., Macdonald F. A., Knoll A. H. and Johnston D. T. (2015b) Statistical analysis of iron geochemical data suggests limited late Proterozoic oxygenation. *Nature* **523**, 451–454.

Stylo M., Neubert N., Wang Y., Monga N., Romaniello S. J., Weyer S. and Bernier-Latmani R. (2015) Uranium isotopes fingerprint biotic reduction. *Proc. Natl. Acad. Sci. U. S. A.* **112**, 5619–5624.

Tribovillard N., Algeo T. J., Lyons T. and Riboulleau A. (2006) Trace metals as paleoredox and paleoproductivity proxies: an update. *Chem. Geol.* **232**, 12–32.

van Maldegem L. M., Sansjofre P., Weijers J. W. H., Wolkenstein K., Strother P. K., Wormer L., Hefter J., Nettersheim B. J., Hoshino Y., Schouten S., Sinninghe Damste J. S., Nath N., Griesinger C., Kuznetsov N. B., Elie M., Elvert M., Tegelaar E., Gleixner G. and Hallmann C. (2019) Bisnorgammacerane traces predatory pressure and the persistent rise of algal ecosystems after Snowball Earth. *Nat. Commun.* **10**, 476.

Vinther J., Stein M., Longrich N. R. and Harper D. A. (2014) A suspension-feeding anomalocarid from the Early Cambrian. *Nature* **507**, 496–499.

Voegelin A. R., Pettke T., Greber N. D., von Niederhäusern B. and Nägler T. F. (2014) Magma differentiation fractionates Mo isotope ratios: evidence from the Kos Plateau Tuff (Aegean Arc). *Lithos* **190–191**, 440–448.

Wang D., Ling H. F., Struck U., Zhu X. K., Zhu M., He T., Yang B., Gamper A. and Shields G. A. (2018) Coupling of ocean redox and animal evolution during the Ediacaran-Cambrian transition. *Nat. Commun.* **9**, 2575.

Wang Z., Lee S. W., Catalano J. G., Lezama-Pacheco J. S., Bargar J. R., Tebo B. M. and Giammar D. E. (2013) Adsorption of uranium(VI) to manganese oxides: X-ray absorption spectroscopy and surface complexation modeling. *Environ. Sci. Technol.* **47**, 850–858.

Weber T., John S., Tagliabue A. and DeVries T. (2018) Biological uptake and reversible scavenging of zinc in the global ocean. *Science* **361**, 72–76.

Wen H., Fan H., Zhang Y., Cloquet C. and Carignan J. (2015) Reconstruction of early Cambrian ocean chemistry from Mo isotopes. *Geochim. Cosmochim. Acta* **164**, 1–16.

Weyer S., Anbar A. D., Gerdes A., Gordon G. W., Algeo T. J. and Boyle E. A. (2008) Natural fractionation of $^{238}U/^{235}U$. *Geochim. Cosmochim. Acta* **72**, 345–359.

Wille M., Nägler T. F., Lehmann B., Schröder S. and Kramers J. D. (2008) Hydrogen sulphide release to surface waters at the Precambrian/Cambrian boundary. *Nature* **453**, 767–769.

Xiang L., Schoepfer S. D., Zhang H., Cao C.-Q. and Shen S.-Z. (2018) Evolution of primary producers and productivity across the Ediacaran-Cambrian transition. *Precambr. Res.* **313**, 68–77.

Xu L. G., Lehmann B., Mao J. W., Qu W. J. and Du A. D. (2011) Re-Os age of polymetallic Ni-Mo-PGE-Au mineralization in Early Cambrian black shales of south China-A reassessment. *Econ. Geol.* **106**, 511–522.

Yang C., Li X. H., Zhu M. Y., Condon D. J. and Chen J. Y. (2018) Geochronological constraint on the Cambrian Chengjiang biota, South China. *J. Geol. Soc.* **175**, 659–666.

Yang J., Barling J., Siebert C., Fietzke J., Stephens E. and Halliday A. N. (2017) The molybdenum isotopic compositions of I-, S- and A-type granitic suites. *Geochim. Cosmochim. Acta* **205**, 168–186.

Yang R., Wei H., Bao M., Wang W., Wang Q., Zhang X. and Liu L. (2008) Discovery of hydrothermal venting community at the base of Cambrian barite in Guizhou Province, Western China: implication for the Cambrian biological explosion. *Proc. Nat. Sci.* **18**, 65–70.

Yeasmin R., Chen D., Fu Y., Wang J., Guo Z. and Guo C. (2017) Climatic-oceanic forcing on the organic accumulation across the shelf during the Early Cambrian (Age 2 through 3) in the mid-upper Yangtze Block, NE Guizhou, South China. *J. Asian Earth Sci.* **134**, 365–386.

Zheng Y., Anderson R. F., van Geen A. and Fleisher M. Q. (2002) Preservation of particulate non-lithogenic uranium in marine sediments. *Geochim. Cosmochim. Acta* **66**, 3085–3092.

Zhu M.-Y. (2010) The origin and Cambrian Explosion of animals: fossil evidences from China. *Acta Palaeontol. Sinica* **49**, 269–287.

Zhu M.-Y., Babcock L. E. and Peng S.-C. (2006) Advances in Cambrian stratigraphy and paleontology: Integrating correlation techniques, paleobiology, taphonomy and paleoenvironmental reconstruction. *Palaeoworld* **15**, 217–222.

Zhu M., Zhang J., Steiner M., Yang A., Li G. and Erdtmann B. D. (2003) Sinian-Cambrian stratigraphic framework for shallow- to deep-water environments of the Yangtze Platform: an integrated approach. *Proc. Nat. Sci.* **13**, 951–960.

*Associate editor:* Alex Dickson